

Resources

Characterising native forest structure from co-incident terrestrial and airborne LiDAR

Project number: PNC546-2021

February 2023



Level 11, 10-16 Queen Street
Melbourne VIC 3000, Australia
T +61 (0)3 9927 3200 E info@fwpa.com.au
W www.fwpa.com.au



**Forest & Wood
Products Australia**

Characterising native forest structure from co-incident terrestrial and airborne LiDAR

Prepared for

Forest & Wood Products Australia

by

**Final Report Editors
Christine Stone and Sam Hislop**

Forest Science, NSW Department of Primary Industries - Forestry



Publication: Characterising native forest structure from co-incident terrestrial and airborne LiDAR

Project No: PNC546-2021

IMPORTANT NOTICE

This work is supported by funding provided to FWPA by the Department of Agriculture, Fisheries and Forestry (DAFF).

© 2023 Forest & Wood Products Australia Limited. All rights reserved.

Whilst all care has been taken to ensure the accuracy of the information contained in this publication, Forest and Wood Products Australia Limited and all persons associated with them (FWPA) as well as any other contributors make no representations or give any warranty regarding the use, suitability, validity, accuracy, completeness, currency or reliability of the information, including any opinion or advice, contained in this publication. To the maximum extent permitted by law, FWPA disclaims all warranties of any kind, whether express or implied, including but not limited to any warranty that the information is up-to-date, complete, true, legally compliant, accurate, non-misleading or suitable.

To the maximum extent permitted by law, FWPA excludes all liability in contract, tort (including negligence), or otherwise for any injury, loss or damage whatsoever (whether direct, indirect, special or consequential) arising out of or in connection with use or reliance on this publication (and any information, opinions or advice therein) and whether caused by any errors, defects, omissions or misrepresentations in this publication. Individual requirements may vary from those discussed in this publication and you are advised to check with State authorities to ensure building compliance as well as make your own professional assessment of the relevant applicable laws and Standards.

The work is copyright and protected under the terms of the Copyright Act 1968 (Cwth). All material may be reproduced in whole or in part, provided that it is not sold or used for commercial benefit and its source (Forest & Wood Products Australia Limited) is acknowledged and the above disclaimer is included. Reproduction or copying for other purposes, which is strictly reserved only for the owner or licensee of copyright under the Copyright Act, is prohibited without the prior written consent of FWPA.

ISBN: 978-1-922718-21-1

Contributing authors: Sam Hislop, John Samuel, Masoomah Alaibakhsh, Christine Stone (NSW Department of Primary Industries); **Susana Gonzales, Perry Han** (Interpine Innovation); **Ruizhu Jiang** (VicForests); **James McGlade, Sven Huettermann** (RMIT).

Forest & Wood Products Australia Limited
Level 11, 10-16 Queen St, Melbourne, Victoria, 3000
T +61 3 9927 3200 F +61 3 9927 3288
E info@fwpa.com.au
W www.fwpa.com.au

Executive Summary

This collaborative, 12-month scoping study was developed in response to the increasing demands for managers to monitor and report on the sustainable management of native forests. A key mechanism for meeting these responsibilities is through quantitative and affordable monitoring of forest condition, including composition and structure. However, the large areas of native forest in Australia necessitate implementing hierarchical multi-source sampling designs, which link tree- and plot-level measurements to airborne and satellite acquired data. The fusion of Airborne Lidar Scanning (ALS) data with Mobile Laser Scanning (MLS) data could help meet these needs. This study aimed to evaluate the capacity of MLS data, acquired using a Hovermap (Emesent) unit, to provide quantified 3D structural information at the tree- and plot-level in six mixed-forest plots located in north-eastern NSW. A comparison was made between traditional manual tree and plot assessments and metrics derived from the Hovermap point cloud data. In addition, the acquisition of co-incident ALS data enabled a comparison of vertical profiles and metrics with the MLS data.

Even with the challenging forest structure present in the field plots (e.g., dense understorey), this study demonstrates that both MLS and ALS point clouds can provide a higher accuracy than traditional field assessment for many plot-level structural attributes. Both lidar datasets produced very similar canopy height models, however, errors with respect to stem counts, particularly for smaller diameter trees, were observed. Nonetheless, when trees detected in the Hovermap data were manually matched with individual trees from the field data, close correspondence in tree height and DBH was obtained, especially for the larger trees ($DBH > 30$ cm). In this study, we present a significant improvement to the automated detection of individual trees in the MLS point clouds by initially classifying tree crowns as overstorey, sub-canopy crowns or standing stag or dead-top trees. A novel tree detection and segmentation algorithm workflow was applied, resulting in significantly improved tree crown delineation and estimates of tree heights and DBH.

Our comparison of the ALS and Hovermap point clouds show that the datasets are complimentary, due to one system operating from above and one from below. Although there are challenges to integrating these point clouds, due to significant differences in pulse densities, it is possible to improve the structural description of subcanopy vegetation by integrating these data. The MLS can be considered a sampling tool, enhancing the efficiency and accuracy of field measurements in native forests. The derived metrics could then be used for spatial modelling to impute traditional inventory metrics or incorporated into biomass, habitat, or wildfire risk modelling across the full ALS extent (and potentially across broader areas with satellite optical and lidar information). The MLS may also prove useful for collecting multi-temporal reference information such as post-disturbance recovery for training and validating broad scale mapping.

It is recommended that a study comparing coincident TLS and Hovermap MLS data be undertaken to provide greater insight into the accuracy of the Hovermap for quantifying tree- and plot-level structural attributes. In particular, further work is required to identify the error source and type associated with estimated parameters of small trees ($DBH > 30$ cm) in the

presence of dense understorey vegetation. Having a survey-grade representative 3D dataset (i.e., TLS) to act as a truth would also allow for an investigation into possible error sources, such as the walking path, walking pace and loop closure points used when moving the Hovermap through the plot. This would also provide greater understanding of occlusion from the presence of understorey vegetation. This information would help guide recommendations for optimising the quality and precision of tree- and plot-level metrics extracted from the MLS and ALS point cloud data.

Table of Contents

Executive Summary	1
Table of Contents	3
Introduction	5
Issues with TLS /MLS point cloud data.....	7
Multisource integrated forest monitoring.....	9
Project aims	10
Methodology	11
Plot descriptions	11
Manual plot measurements.....	15
Lidar data.....	17
Hovermap data acquisition and processing.....	17
Airborne laser scanning data acquisition and processing.....	19
Tree-level analyses.....	19
Manual comparison of field and Hovermap tree-level measurements.....	19
Evaluation of the FSCT to extract tree-level attributes from Hovermap data	20
The detection of tree-level subcanopy vegetation in ALS data	20
Plot-level analyses.....	21
Voxel size.....	21
Plot-level vertical distribution vegetation patterns using Hovermap data	21
Plot-level lidar metrics	22
Evaluation and comparison of vertical profiles for Hovermap and ALS data	22
Comparison of ALS and MLS cover estimates.....	23
Derivation of fuel hazard metrics and fuel connectivity using Hovermap data.....	23
Evaluation of GEDI data for characterising forest structure changes following wildfire....	24
Project data management	25
Results	26
Tree-level analyses.....	26
Manual comparison of field and Hovermap tree-level measurements.....	26
Evaluation of the FSCT to extract tree-level attributes from Hovermap data	27
Comparison of DBH and tree height between field measurements and FSCT outputs ...	28
Height estimates using the tree level PAD profiles.....	30
Standing stag or dead-top tree detections using MLS data	31
Summary of crown types extracted from the Hovermap data from the 3 plots	32
Detection of tree-level subcanopy vegetation in ALS data.....	33
Plot-level analyses.....	34
Summary of field measurements presented at a plot level or per hectare basis.....	34
Comparison of inventory stem counts/ha and basal area with Hovermap derived estimates (Interpine Innovation).....	35
Comparison of the ALS and Hovermap MLS data	36
Derivation of fuel hazard metrics and fuel connectivity using Hovermap data.....	41
Evaluation of GEDI data for characterising forest structure changes following wildfire....	43
Discussion	45
Tree-level analyses.....	45
Plot level analyses	46
Fuel assessments	48

Fusion of point clouds from multiple platforms.....	48
Future research	49
Conclusions	50
Recommendations	51
References	52
Acknowledgements	57

Introduction

Over the past 20 years, forest resource management has been one of the main driving forces in the operational adoption of airborne laser scanning (ALS). However, due to the recognition that native forests provide ecological and social ecosystem services in addition to economic benefits from timber extraction, there is increasing demand for quantitative information on the condition and ecological status of native forests (Coops *et al.* 2022). Successful sustainable management of native forests requires detailed information on forest structural diversity and composition, where structural diversity explains the arrangement and distribution of the structure of vegetation elements (Donager *et al.* 2021). Therefore, accurate and timely retrieval of vegetation structure metrics is now a key component of management, monitoring and reporting activities undertaken by forest managers.

Lidar data acquired by aircraft can cover forests at the estate-level and provide information related to the structural conditions covered by the dominant canopy and largest trees (i.e., as seen from above). ALS data is now frequently used operationally for plot imputation to create wall-to-wall estimates of inventory metrics (White *et al.* 2013). ALS data can also be used directly to derive a suite of stand level metrics including canopy height, cover and texture (e.g., Niemi & Vauhkonen 2016).

While some authors have reported that ALS may not fully capture the vertical distribution of vegetation in complex multilayered and dense forests due to the attenuation of the laser pulses (Giannetti *et al.* 2018), vertical profiling using ALS data has been demonstrated in some native forests (e.g., Wilkes *et al.* 2016; Crespo-Peremarch *et al.* 2020). Jiang (2020), for example, extracted height percentiles and the density of points within height classes to provide canopy profile models for comparison of eucalypt forest structure in the Central Highlands of Victoria. The density of points was assumed to represent foliage density in different height strata and used to examine the connectivity between vertical layers. Thus, in addition to predicting traditional inventory metrics, ALS data is now being applied to quantify a broader suite of forest stand assessments including habitat suitability (e.g., Ciuti *et al.* 2018, Bakx *et al.* 2019, Carrasco *et al.* 2019, Jiang 2020); canopy change detection (disturbance / recovery) (Karma *et al.* 2020); above ground biomass estimates (e.g., Kim *et al.* 2016) and wildfire modelling / fuel load estimation (Price & Gordon 2016). Depending on the point density and complexity of the forest canopy, ALS has also been applied to locate individual tree crowns (e.g., Ene *et al.* 2012; Kandare *et al.* 2016; Aubry–Kientz *et al.* 2019).

Estimation and mapping of inventory parameters require tree scale measurements from field reference plots located within a representative sampling design (Liang *et al.* 2018, Tompalski *et al.* 2021). These measurements can be employed to train, calibrate and/or validate spatial models that scale up to areas covered by remotely sensed data. Forest structural elements have traditionally been assessed by manual field inventories. While the tree level measurements of tree density, stem diameter and tree height can be reliably obtained by field crew, estimates of plot level structural attributes such as understorey density and cover, are often inaccurate, imprecise, and time-consuming. Ashcroft *et al.* (2014) reported a large variation between observers working in native eucalypt stands, partly due to misjudging the height of vegetation.

ALS, if acquired at a relatively high point density (> 10 points/m²) and over forests with homogenous canopy (without interlocking crowns and suppressed trees), can be used to derive accurate tree heights and locate and delineate individual tree crowns. Acquiring ALS data at greater than 20 pulses/m², Corrao *et al.* (2022) achieved acceptable tree-level estimates of Diameter at Breast Height (DBH) and volume in a *Pinus taeda* plantation compared to conventional cruised measurements. However, ALS is limited in its capacity to directly measure parameters like DBH because of the sensor being positioned above the canopy. Terrestrial (TLS) and mobile laser scanning (MLS), on the other hand, are positioned below the canopy and are receiving considerable attention as an alternative approach to manual field collection (Hyypä *et al.* 2020; Coops *et al.* 2022). Both platforms allow for much higher point densities below the forest canopy compared to ALS and are assumed to be the best available information to describe finer subcanopy elements, providing information with a ‘bottom up’ perspective (Crespo-Peremach *et al.* 2020). The analysis of TLS data to estimate tree-scale attributes has made significant advances with the estimation of tree stem parameters principally focused on circle / cylinder fitting algorithms (e.g., Pitkänen *et al.* 2019). Numerous individual tree segmentation algorithms using dense point cloud data have now been published. For example, application of the random sample consensus (RANSAC) cylinder fitting algorithm (e.g., Hyypä *et al.* 2020, Donager *et al.* 2021, Liu *et al.* 2021) and several open-source packages are now available (e.g., Krisanski *et al.* 2021, Wilkes *et al.* 2022). Krisanski *et al.* (2021) developed the Forest Structural Complexity Tool (FSCT), which is a robust, sensor agnostic and fully automated approach to extracting detailed tree structural attributes (e.g., tree location, DBH and height) from dense point clouds.

Registration of multiple TLS scans can be achieved with the use of retro-reflective targets as tie-points (e.g., Styrofoam spheres or reflective ground control points) and finer registration can be achieved using software, which can also remove ‘noise’. However, occlusion remains a major issue with static TLS (e.g., Donager *et al.* 2021). Occlusion is the fact that some stems, branches, and leaves may not be scanned as they are hidden by elements closer to the scanner. The use of TLS, therefore, requires a plot to be scanned from multiple locations using accurately positioned tie-points for the scan co-registration process to form a single point cloud. This can be a time-consuming task.

More recently, MLS is proving to be a useful tool for rapid assessment and monitoring, especially in forests and plantations that present a relatively simple stand structure (Gollob *et al.* 2020, Hyypä *et al.* 2020, Bienert *et al.* 2021, Stal *et al.* 2020). MLS techniques can be divided into vehicle-based scanning, unmanned aircraft (UAV), hand-held and other personal scanning techniques, including backpack MLS.

MLS systems adds the aspect of movement along a track (trajectory) to static TLS acquisition methods. They can reduce tree level inaccuracies created by occlusion by incorporating many views during data collection as well as increasing the areas scanned (Donager *et al.* 2021; Mokos *et al.* 2021). Interpine Innovation have purchased two MLS units to enhance their inventory capacity (<https://interpine.nz/adding-the-emesent-hovermap-slam-lidar-solution-to-our-services/>). Recently there has also been the release of colour and depth sensors (RGB-D) that have been integrated into consumer devices such as smartphones and tablets. These devices can be used outdoors and operate in a similar manner to MLS to reconstruct 3D

scenes in near real time. However, they offer a lower spatial resolution and effective range (dependant on depth sensor technology) when compared to conventional MLS. For example, the iPad Pro has an active projection RGB-D sensor with an effective range of < 5 m (Cakir *et al.* 2021).

A significant advantage of MLS technology is the removal of the need for accurate Global Navigation Satellite System (GNSS) signals (which can be disrupted by forest canopy) through the adoption of Simultaneous Location and Mapping (SLAM) technology (Gollob *et al.* 2020). SLAM algorithms operate by using a combination of feature detection algorithms and motion data captured with an Inertial Measurement Unit (IMU) to estimate the location of features relative to the sensor. However, one challenging issue of native forest environments is that the objects have less clearly defined edges, which means that the SLAM algorithm can find it more difficult to accurately co-register objects. In general, MLS data tend to be ‘noisier’ than fixed location TLS data, resulting in a more ‘fuzzy’ point cloud (Gollob *et al.* 2020, Donager *et al.* 2021; Mokos *et al.* 2021).

Several studies have demonstrated that MLS data can produce more accurate estimates of tree-level attributes such as DBH compared to ALS data (e.g., Giannetti *et al.* 2018). Interpine Innovation now have operational workflow solutions for remotely obtaining tree diameter and height measurements in *Pinus radiata* plantations using the point cloud data acquired by a Hovermap unit. Their data workflow applies deep learning algorithms for stem detection and segmentation. Far fewer studies have used MLS data for individual tree stem curve and volume (Hyyppa *et al.* 2020). Interpine Innovation and Drs Winyu Chinthamit (University of Tasmania) and Mitch Bryson (University of Sydney) have significantly progressed assessments of stem sweep and stem features of plantation trees by importing segmented trees into a Virtual Reality environment for visual and on-screen measurements (FWPA PNC520-1920 ‘Operational immersive visualisation and measurement of dense point cloud data in forest inventory’).

The range of the MLS scanner and the density of the point cloud depends on many factors: (1) stand characteristics, in particular stand density, tree species and age structure of the trees, as well as density and height of the understorey vegetation; and (2) technical features of the mobile mapping system, in particular the scan rate, speed of the platform and the precision of the trajectory (Bienert *et al.* 2021). Therefore, parameter accuracies are significantly influenced by the survey path followed by the user during data acquisition. Errors can be reduced by ‘closing the loop’ in the path survey (Gollob *et al.* 2020, Stal *et al.* 2021). The principal of loop closing is to minimize the ‘positional drift’ in the MLS IMU/SLAM process.

Issues with TLS /MLS point cloud data

There are several categories of descriptive, stand level ALS metrics based on canopy height, cover and density across height strata (e.g., Pearce *et al.* 2019, Fisher *et al.* 2020) that are now used routinely for the prediction of tree- and plot-level attributes. Many of these metrics can also be extracted from MLS data (e.g., Liu *et al.* 2017), however, the higher resolution of MLS, particularly at the terrestrial level that is often occluded in ALS, also enables additional plot-level metrics relating to stand structural complexity (e.g., Van Ewijk 2015, Ehbrecht *et al.* 2016, Tompalski *et al.* 2015; Atkins *et al.* 2018).

Unlike ALS data, which presents a consistent nadir perspective, TLS / MLS data are characterized by non-uniform point densities, because density is influenced by the distance to the objects and the speed of the MLS capture. The raw ground-based lidar points are biased towards proximity to the scanner. There are also issues associated with beam divergence; the higher beam divergence of MLS instruments reduces the penetration of the laser through the understorey compared to TLS scanners. The segmentation of forest MLS data is therefore challenging, as variable point density, together with occlusion, impacts the quality of the tree segmentation result. In addition, many of the structural complexity metrics require spatially homogeneous point clouds.

One approach to manage the heterogenous high density of MLS data is through the application of voxels (Kim *et al.* 2016, Sumnall *et al.* 2016, Juchhelm *et al.* 2017, Zhang *et al.* 2017, Pearce *et al.* 2019, Calders *et al.* 2020). Using this approach, the point cloud is partitioned along both the vertical and horizontal axes to form volumetric pixels (i.e., voxels). Voxel-based metrics are then created by operating on or summarising the lidar points that fall within each voxel (Pearce *et al.* 2019). Metrics can be related to the number of lidar returns falling within each voxel, which is directly influenced by the chosen voxel dimensions. The voxel space can be simplified to approximate occupancy by classifying each voxel as empty / not empty based on the presence or absence of returns within each voxel (i.e., a binary voxel model indicating vegetation presence or absence). Ehbart *et al.* (2016), for example, presented the standardized plot metric ‘effective number of layers (ENL)’ as a measure of vertical stand structure. The vertical structure is stratified into layers of 1 m thickness and the number of populated voxels with a side length of 20 cm inside each layer is counted. The ENL is then computed using the inverse Simpson diversity Index. For the ENL, increasing stand height and a more even occupation along the vertical profile result in higher values.

Voxelization has also been applied to derive compound structural parameters. For example, Hillman *et al.* (2021) utilized a binary voxel model derived from TLS data acquired in a dry sclerophyll forest to estimate vegetation cover at critical height thresholds and quantify ladder fuel as an approach to assess fire hazard.

An important decision is to determine the appropriate voxel size. This can be made based on a preliminary investigation of multiple voxel size permutations (Kim *et al.* 2016). Another decision that is often considered is whether to utilise all of the return points, or only those labelled by ‘Return number’ as either first returns (the majority of points) or secondary or other returns (which tend to have weaker intensities). These decisions are considered in this project to reduce data volume and to harmonize the differing point densities acquired from MLS and ALS platforms.

A key step to integrating ALS and MLS point clouds is their registration to common spatial alignment. However, the issue of accurately positioning and co-registering MLS point clouds with manually measured reference trees or other point cloud datasets (e.g., ALS) can be challenging. Commercial software provided by the MLS instrument providers (e.g., GeoSLAM software) processes the data automatically and can register multiple 3D point clouds using MLS IMU data and feature detection algorithms. Initially, coarse registration of scans is achieved by identifying common points within the plot. The point cloud coordinates are first assigned to a local reference system, with the start position of the walking path being

fixed at triple zero for the X, Y, and Z coordinates (Gollop *et al.* 2020). A common approach to co-register multiple point cloud datasets is to use software such as Cloud Compare. The point cloud can be rotated and translated using known geo-positioned reference points and converted from the local coordinate system to a global coordinate system.

In addition to the extraction of plot-level structural attributes, numerous studies have successfully segmented individual tree stems using TLS, and more recently, MLS point clouds. However, while these algorithms have proven robust for uniform stems as occur in plantations, inaccuracies increase with trees having irregular stem features and the presence of dense understorey vegetation. (Kankare *et al.* 2015; Liang *et al.* 2018; Stal *et al.* 2021; Vatandaşlar & Zeybek 2021).

Many of these algorithms can be accessed in open software packages such as lidR (<https://cran.r-project.org/web/packages/lidR/index.html>) (Roussel J.-R. *et al.* 2020), forestrR (<https://cran.r-project.org/web/packages/forestr/index.html>), LAStools (rapidlasso.com) and the Forest Structural Complexity Tool (<https://github.com/SKrisanski/FSCT>).

Multisource integrated forest monitoring

The concept of an integrated, multi-source, multi-scale framework for monitoring large areas of native forest is becoming a reality through the adoption of rapidly advancing remote sensing technology such as lidar (Figure 1; Coops *et al.* 2022, Sofia *et al.* 2022). However, integrating ALS data with plot-level, sub-canopy TLS or MLS has received limited attention. In one study, Lui *et al.* (2017) produced canopy height profiles (CHP) from TLS data based on the number of filled voxels at every 0.1 m layer of forest and from ALS using the percentile distribution of returns every layer at 0.5 m intervals. They then selected values from both CHPs for spatial modelling.

The next level of data fusion in such a monitoring framework is the integration of airborne data (e.g., ALS) with data acquired by spaceborne sensors that cover large areas. An example of spaceborne lidar is Global Ecosystem Dynamics Investigation (GEDI) instrument onboard the International Space Station, which has been collecting data since April 2019. A description of the GEDI system and data acquisition specifications are presented in Spracklen & Spracklen (2021). GEDI is designed to provide high-resolution observations of forest vertical structure. Currently the data are being used to create a suite of vegetation structure and biomass products, including vegetation height and cover (Potapov *et al.* 2021). However, GEDI is a sampling instrument and as such wall-to-wall products are being derived through integration with optical data such as Landsat. ALS data can be used to provide the training data for GEDI-based spatial models (e.g., Dorado-Roda *et al.* (2021).

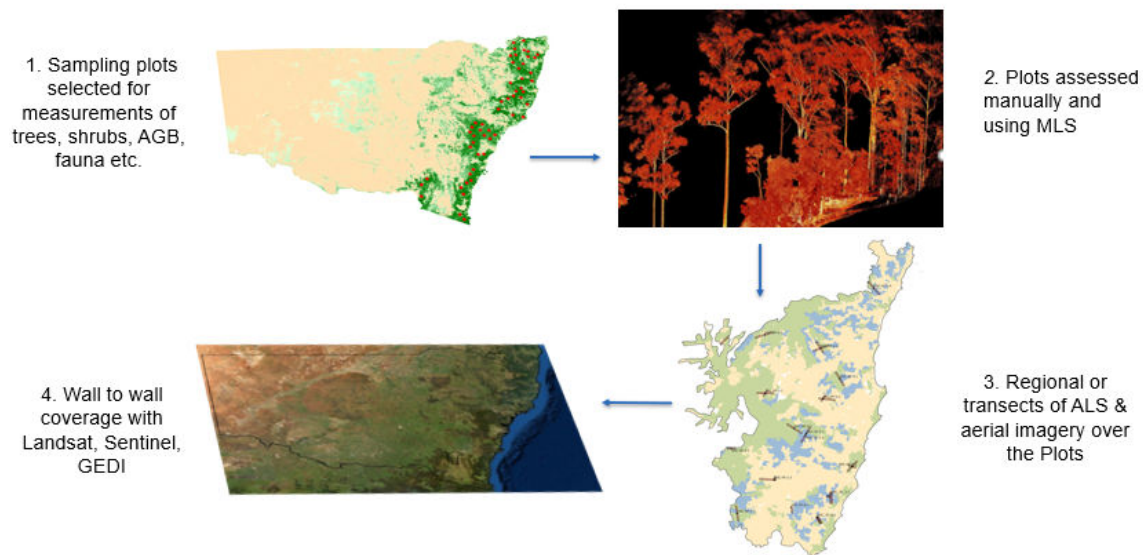


Figure 1. Possible multi-phase, hierarchical sampling design for an integrated monitoring system for native forests – illustrated for NSW.

Project aims

This collaborative, 12-month scoping study aimed to evaluate the capacity of MLS (Hovermap) data to provide quantified information characterising the complex vertical and horizontal structure in different eucalypt forest types, at both the tree- and plot-level, located in north-eastern NSW. The acquisition of co-incident ALS data allowed for a detailed comparison of derived vertical profiles and metrics, which is needed to better understand the commonalities and differences in how these data represent forest structure. While both systems are based on lidar, the different position of the sensor in relation to the forest canopy leads to different outputs. Understanding the strengths and weaknesses of different remote sensing systems is essential prior to forming conclusions about forest structure.

The objectives pursued in this study were to:

- determine the suitability of MLS (Hovermap) 3D data in characterising the vertical and horizontal spatial patterns in plots presenting differing stand structure and forest types
- demonstrate the capacity of Hovermap data to estimate tree- and plot-level inventory parameters in native forests
- identify and compare structural metrics extracted from dense point cloud data acquired from MLS (Hovermap) and ALS platforms
- identify metrics and more complex parameters derived from MLS data potentially suitable for training and validation of ALS based spatial models
- undertake a preliminary evaluation of spaceborne lidar GEDI data to detect short-term structural changes in native forests following wildfire.

This study has leveraged another study funded by NSW Local Land Services and managed by the Forest Science team within NSW Department of Primary Industries. As all the field plots established for these two projects are located in native forests on private property, the precise location information has been ‘desensitised’ and remains confidential.

Methodology

Plot descriptions

The field plots for this study were located on six private property forests which were established as part of a larger NSW DPI and NSW Local Land Service (NSW LLS) project. Each property has a current NSW private native forestry vegetation plan (PNF PVP; i.e., a plan authorising timber harvesting). The precise location of the plots is confidential as required in a Licence Data Agreement with NSW LLS. Each plot was given a unique identifying code. The selection of these plots was based on a sampling design developed by Dr Amrit Kathuria (DPI Forest Science Biometrician). The plots were in stands covered by a PNF PVP and in areas that were not identified as exclusion areas (slopes exceeding 25 degrees, close proximity to riparian areas or rocky outcrops or areas containing old regrowth or rainforest).

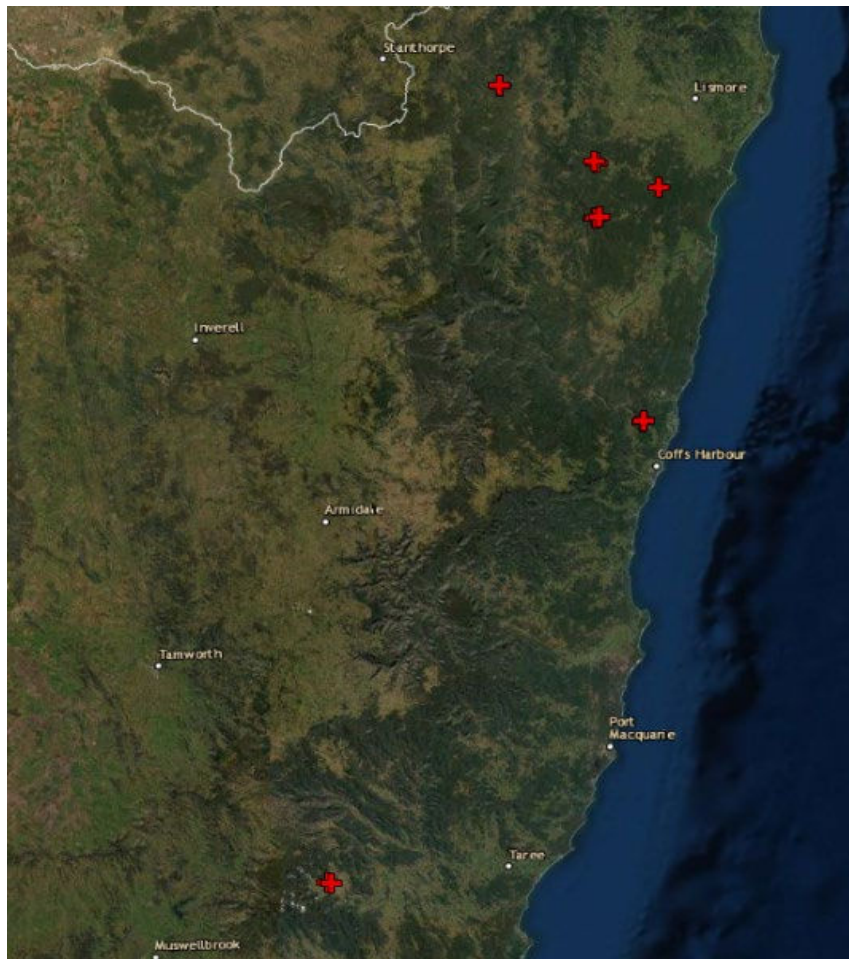


Figure 2. Location of plots in the mid and upper North Coast of NSW

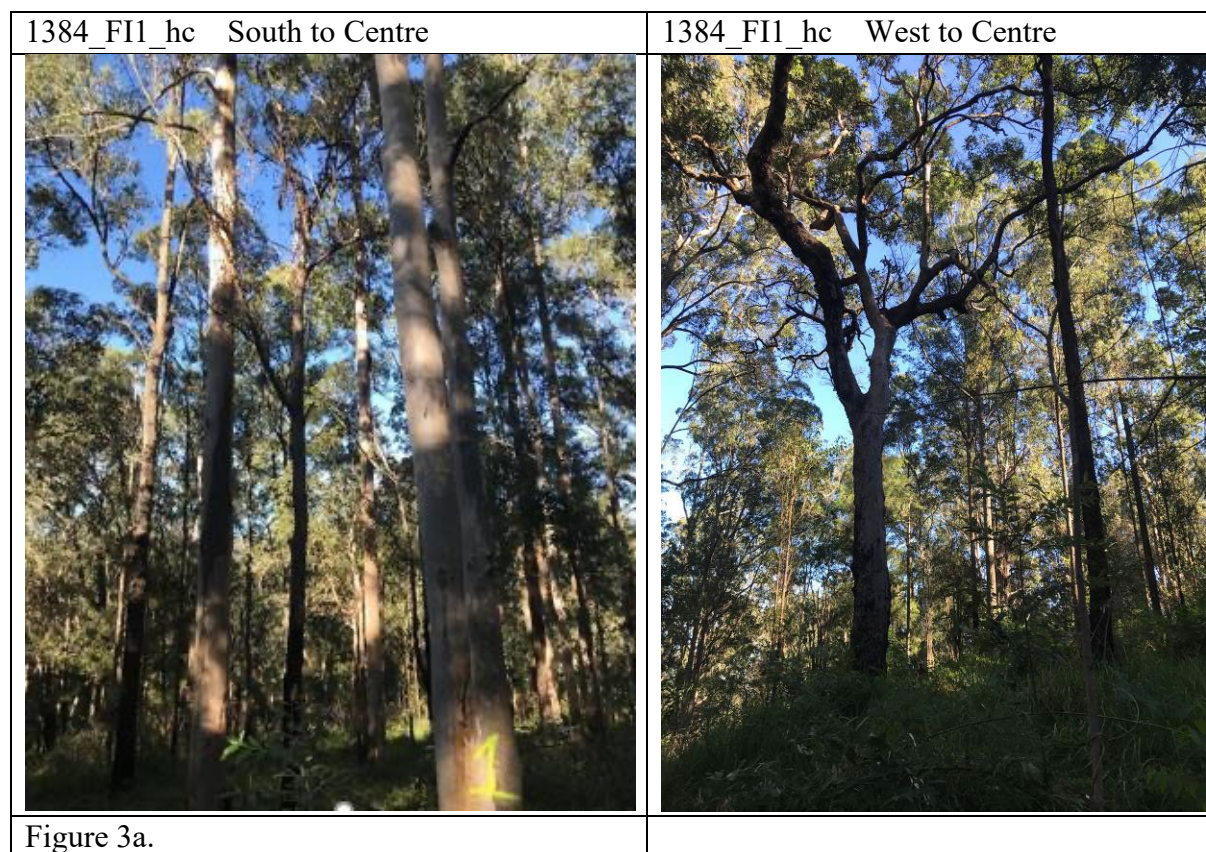
A ‘fully monitored’ plot was established on each property during May 2021. A further two to three inventory plots were established on each property by Forestry Corporation of NSW (FCNSW) field inventory staff during May – August 2021, providing a total of 13 plots. 11 plots were scanned with the Hovermap. A summary of the six monitoring plots is shown in Table 1.

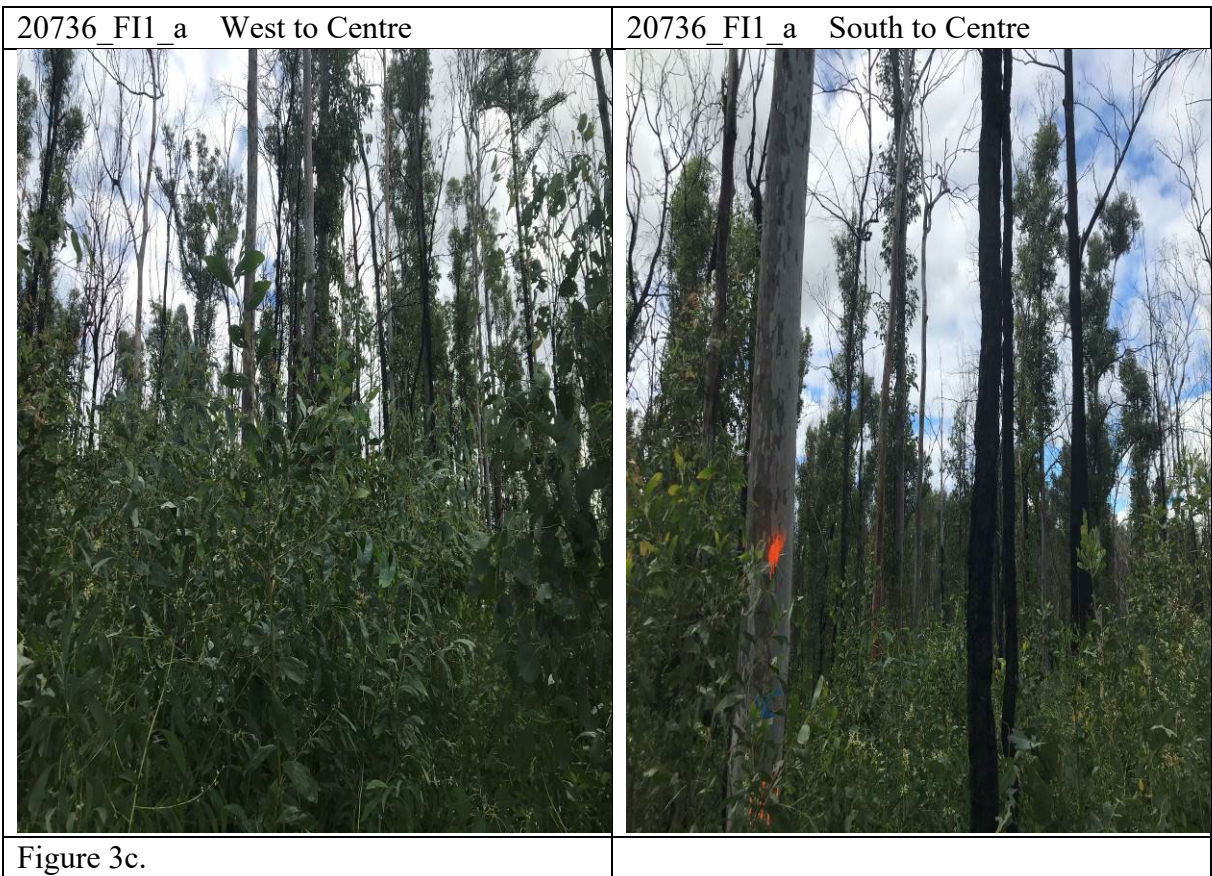
Table 1. Plot descriptions for the six fully monitored plots

'Fully monitored' Plot ID	1384_FI1_hc	18553_I0_a	20736_FI1_a	25703-02_FI1_bc	26412_FI1_ec	26739_I0_a
Slope (Degrees)	8	1	10	3	23	25
Large tree Plot radius (m)	17.93	17.84	17.98	17.85	18.60	18.74
Slope adjusted Plot area (ha)	0.101	0.100	0.102	0.100	0.109	0.110
Aspect - Degrees magnetic	344	197	90	160	175	107
Plot disturbance	Fire Recent Moderate	Fire Recent Light	Fire Recent Severe, Harvesting within view of plot, Thick wattle, Soil erosion	Fire Recent Moderate Harvesting within view of plot	Harvesting within view of plot, Animal grazing	Harvesting in plot boundary, Harvesting within view of plot
Yield Association Group	Dry Sclerophyll Forest	Semi-moist and Taller Dry Eucalypts	Spotted Gum	Moist Coastal Eucalypts	Semi-moist and Taller Dry Eucalypts	Blackbutt

²Baur G.N. (1965) Forest types in New South Wales. Research Note number 17, Forestry Commission of New South Wales

Figure 3. Example photographs from the six fully monitored plots, illustrating the range of differing stand structural conditions





25703-02_FI1_bc North to Centre



Figure 3d.

25703-02_FI1_bc Centre to South

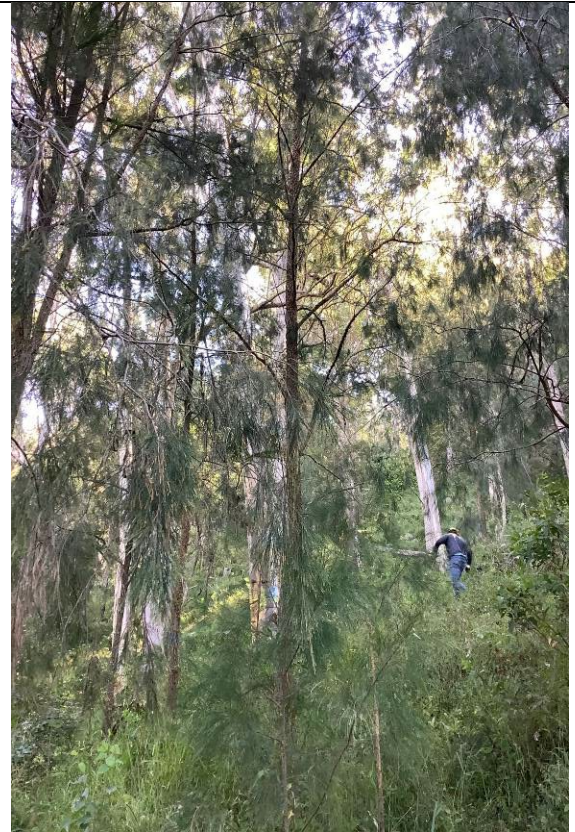


26412_FI1_ec North to Centre



Figure 3e.

26412_FI1_ec South to Centre





Manual plot measurements

The plot data were collected by NSW DPI Forest Science staff, FCNSW inventory crew and a botanist (Birdwing Ecological Services). The plot data were acquired according to a draft Forest Monitoring Manual being prepared by John Samuel (NSW DPI Forest Science) for the NSW LLS PNF project. An outline of the manual is presented in Figure 4 as a suite of modules. Each module has been developed into data collection applications in ESRI Survey 123. Survey 123 can be loaded on any smart device, works off-line, does not require a ESRI ARC GIS licence, integrates with ARC GIS, gathers geo-points and allows the capture of photographs. The application was pre-programmed with drop-down lists, mandatory fields and species look up tables. Once all the plot data were collected, the files were uploaded to the cloud and retrieved by an ESRI licenced analyst.

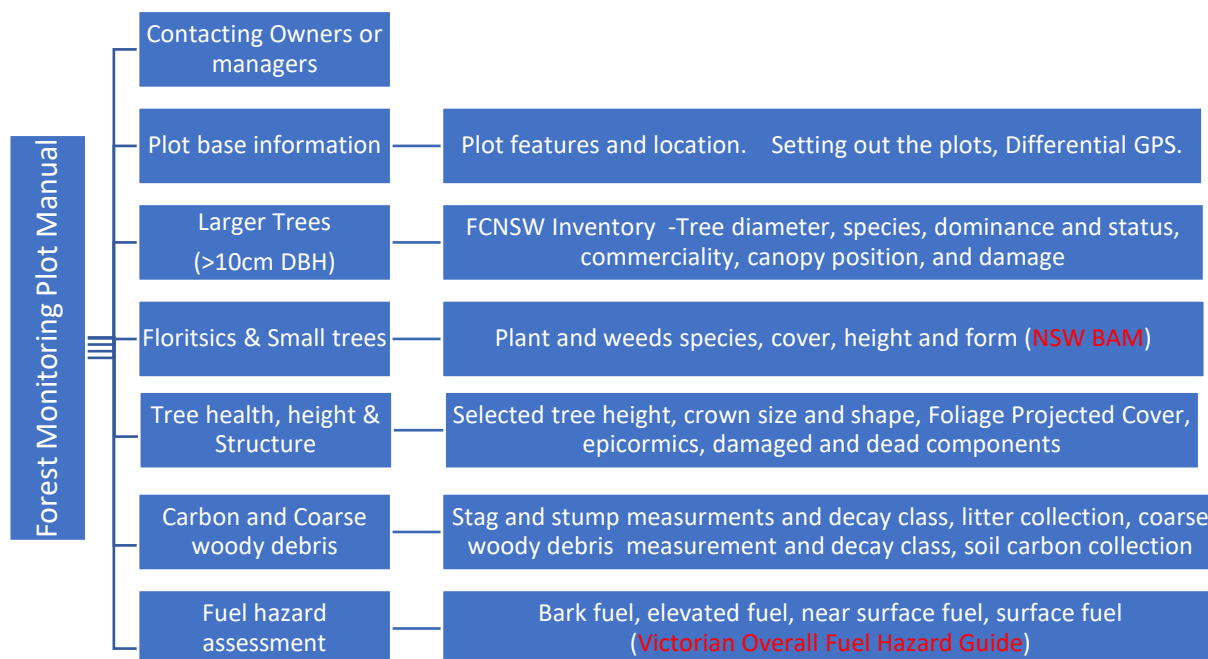


Figure 4. Outline of the PNF Forest Monitoring Manual

The centre of each plot was accurately located using a Trimble dGPS. Each 0.1 ha circular plot was then marked to provide three concentric sub-plots; having radii of approximately 17.84 m for large tree assessment, 11.28 m for growth assessment and 3.99 m for small tree assessment, after their areas were adjusted for slope.

The species and DBHs were recorded for the large trees (DBH > 10cm) in both the fully monitored plots and traditional inventory 0.1 ha plots and each tree was clearly numbered. Small trees were defined as having DBH < 10 cm and height > 1.3 m. The traditional inventory plot/tree parameters were acquired by FCNSW inventory crews and data was recorded using the software package Plot Safe, proprietary software developed by Interpine Innovation (<https://interpine.nz/plotsafe/>). For all trees (DBH > 10cm) recorded attributes included tree diameter, species, dominance and status, tree bearing and distance from the plot centre, commerciality, canopy position and damage. Basal area was calculated from the DBH measurements of these trees. Tree heights were obtained using a vertex for 7 to 12 representative large trees per plot. While plot areas were slope adjusted, analysis of the Hovermap data involved clipping all plots to a radius of 17.84 m irrespective of slope. Therefore, inventory parameters are reported on a per ha level to permit direct comparisons.

A key structural attribute assessed in the fully monitored plots was an estimation of vegetation strata canopy cover. These assessments were done at the plot cardinals and centre point, with visual estimates of lower storey vegetation (> 1.3 m and < 2 m), mid storey (> 2 m and < 10 m), upper storey (> 10 m), with emergent vegetation being those trees whose crowns reached above the upper storey. Average canopy cover (> 1.3 m) per plot was also obtained using the application ‘% Cover’ (<https://percentagecover.com/>). This application uses the device (iPhone / iPad) camera to estimate the proportion of photo filled with leaf and wood when orientated vertically, in our case at the four cardinal points and plot centre.

Plot level estimates of fuel hazard were also obtained through visual estimates of bark fuel, near surface fuel and surface fuel following the methodology provided in the Victorian Overall Fuel Hazard Guide.

Lidar data

Hovermap data acquisition and processing

The Emesent Hovermap (<https://www.emesent.io/hovermap/>) is a lightweight (1.8 kg) mobile unit fitted with a Velodyne Puck (previously VLP-16) lidar scanner which can be handheld, attached to a backpack or mounted to a drone (Figure 5). It utilises real-time processing of 3D SLAM (Simultaneous Localization and Mapping) algorithms to generate 3D point clouds. The unit does not require a GNSS and therefore is not subject to the same challenges as other systems that are dependent on satellite derived positional information. In open areas the Hovermap unit has a lidar range of up to 100 m and a mapping accuracy of +/- 20 mm. The sensor records both strongest returns (return number is 0) and last returns (return number is 1). The number of last returns is about 10% of total returns. For example, for the 01384FI1hc plot, the total number of return 0 points was 89,184,258 and return 1 was 10,016,359.



Figure 5. Interpine Innovation’s backpack Hovermap unit used in the study

Hovermap data was collected in each of the fully monitored plots as well as the additional inventory plots. The datasets were acquired according to instructions provided by Interpine Innovation (David Herries and Susana Gonzalez). The Hovermap survey path started at the centre of each plot and the operator proceeded in a spiral walk, walking at a brisk pace. The

survey aim was to pass most trees within a distance of 3 to 4 m. It is important that each survey start and finish at the same place. In plots on steep ground, Interpine Innovation recommends an extra loop up slope of the plot. The instructions also provide advice on the procedures on setting up the Hovermap unit and how to download the data. Following a scan, the raw data is transferred from the Hovermap computer to a secondary processing computer for computation of the global SLAM solution and final point cloud. Figure 6 presents the processing workflow applied to the MLS datasets. This involves point cloud classification (e.g. identifying points associated with stems and foliage), point height normalisation and then tree segmentation and computation of tree height and diameter.

A novel component of this data workflow involves loading the processed 3D point clouds into a virtual reality environment allowing for supervised deep learning. This approach is now applied operationally by Interpine Innovation for MLS data acquired in pine plantations. The critical attribute of the classification algorithm is the quality of the training datasets for the deep learning approach. The VR screen operator can adjust the tree data inside the VR environment to improve it for subsequent measurements. These training datasets have not yet been acquired for examples of eucalypt species in native forests.

Initially, coordinates of the registered point cloud are represented by a local reference system, with the start position of the walking path being fixed at triple zero for the X, Y, and Z coordinates. The point cloud can then be converted to a global coordinate system to enable co-registration of other spatial datasets (such as the ALS data). The dGPS data was post processed to the GDA2020 datum and MGA zone 56 (EPSG code 7856), which was then used to align the Hovermap data.

Hovermap LiDAR Processing Workflow

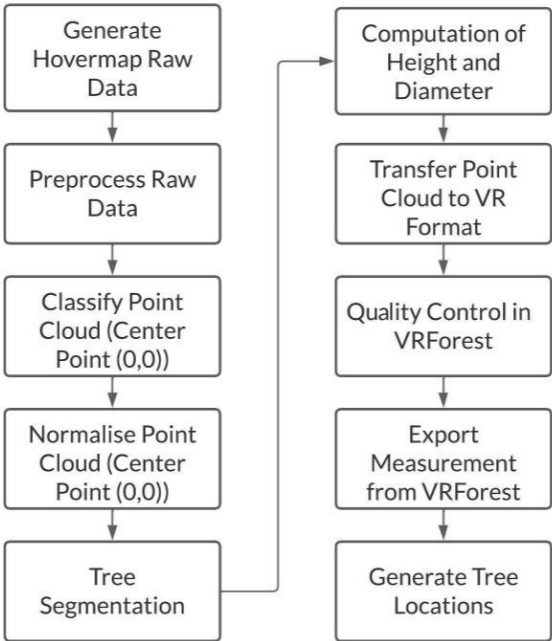


Figure 6. Workflow for the Hovermap lidar data processing undertaken by Interpine Innovation

Airborne laser scanning data acquisition and processing

As part of the LLS PNF project, ALS transects that were spatially coincident with the six PNF properties were acquired by Aerometrex Ltd. in May 2020 and 2021 using a Riegl LMS-Q1560 scanner (Table 2). The discrete multi-return ALS data were acquired at a density of a minimum of 10 pulses / m², with a scan angle of 14° either side of nadir and beam footprint of ≤ 30 cm. In addition to the point cloud data, Aerometrex also provided the associated terrain and surface/canopy height models, along with RGB orthophotography.

Table 2. Number of transects and area covered by ALS data

Property ID	No. of transects (2020)	No. of transects (2021)	ALS coverage (2020) (ha)	ALS coverage (2021) (ha)
01384	4	4	808	925
18553	1	1	35	40
20736	5	4	349	349
25703-02	1	1	98	119
26412	3	3	546	664
26739	1	1	79	83
Total	15	14	1,915	2,180

Tree-level analyses

Manual comparison of field and Hovermap tree-level measurements

A manual comparison of spatially matched trees identified in the field plot measurements and the Hovermap 3D data processed by Interpine Innovation was undertaken for three plots: 01384_FI1_hc, 26412_FI1_ec and Plot 26739_10_a. Trees with the magnetic bearing and distance from the plot centre recorded, as well as DBH and height measurements, were matched with the same trees in the processed Hovermap datasets using ArcGIS Pro. To convert the compass magnetic bearing and distance locations to a GIS point layer, the magnetic bearings were converted to true bearing (degrees clockwise from the North Pole). Initially there appeared to be poor locational correspondence between the datasets. This task was made more difficult as the tree numbering differed between the field and Hovermap datasets. In addition, while the field plot areas were adjusted for slope, the plot areas in the Hovermap datasets were defined by a fixed radius of 17.84 m. It was also assumed that observer error would occur in the bearing and distance field measurements, especially in plots having dense understorey vegetation. The matching of trees was improved by comparing DBH measurements of trees within the same neighbourhood. The neighbourhood height information was augmented by visual assessment of the co-incident ALS CHM raster.

The comparison of tree heights in this study was achieved through two approaches. In the first method, the spatial datasets derived for location and DBH were imported into the open-source software, Cloud Compare. To estimate a Hovermap value, six (highest) nearest neighbour Z points were selected and averaged. Tree heights were also compared using the CHM layers derived from the co-incident ALS and Hovermap point cloud data. The DBH and tree height values of matched trees were then compared.

Evaluation of the FSCT to extract tree-level attributes from Hovermap data

Parallel to the tree level comparison above, the Forest Structural Complexity Tool (FSCT; Krisanski *et al.* 2021) was evaluated in terms of its ability to extract tree level information from the Hovermap data for three plots (1384_FI1_hc, 18553_I0_a and 26412_FI1_ec). Outputs from two of these plots (1384_FI1_hc and 26412_FI1_ec) were used to compare with the field-measured individual tree locations, DBH and tree height. FSCT is a new open-source Python package (available at <https://github.com/SKrisanski/FSCT>) which requires a powerful desktop computer configuration. For this evaluation, the desktop computer used included an Intel Core i7 10700F, 64GB RAM and ASUS GeForce RTX 2070. To evaluate whether processing time could be improved without compromising results, we compared the FSCT outputs between using all Hovermap returns versus last returns only. The aim was to test if using only last returns was sufficient for characterising complex structures in eucalypt forests.

The FSCT uses a deep learning technique to segment a normalised lidar point cloud into four categories: terrain, vegetation (foliage), CWD and stems. Vegetation and stems were then segmented into individual trees and assigned an individual tree ID. In the FSCT, the highest points of each tree are taken as the tree height measurement.

To improve the accuracy of tree height estimates in the FSCT, especially for trees in the sub canopy, a new methodology was developed based on tree-level plant area density (PAD) profiles, which classified trees as either sub canopy or canopy trees and stag or dead top. The PAD at a given height (z) is estimated using the projection coverage of the point cloud at that height level. The PAD is based on the concept of leaf area index (LAI) and gap fraction profiles, and at a given height (z) is estimated using the projection coverage of the point cloud at that height level (Carrasco *et al.* 2019).

This new workflow involved building separate tree-level PAD profiles for three categories: (1) foliage only (PAD_f), (2) stem only (PAD_s) and (3) foliage + stem (PAD_{fs}). Based on the changes of PAD by height, it was possible to identify the height break of the sub-canopy as the minimum density height layer where the plant density is smaller than its the upper- and lower-layer density. The PAD at a given height (z) is estimated using the projection coverage of point clouds at that height level. The shape of PAD_f , PAD_s and PAD_{fs} and the detected sub-canopy height was then used to reclassify the individual trees detected in the Hovermap data into three crown types: Overstorey, sub-canopy, and stag or dead top.

- Overstorey: there is no clear height break in all categories (PAD_f , PAD_s and PAD_{fs})
- Sub-canopy: clear height break identified in both PAD_f , and PAD_s , OR at least one clear height break in PAD_s
- Standing stag or dead-top tree: clear height break identified in PAD_f but no clear height break in PAD_s

The detection of tree-level subcanopy vegetation in ALS data

Individual tree segmentation was also undertaken on the ALS data. For this process, the algorithm used was the marker-control watershed segmentation in the lidR package in R 3.6.3. Tree-level PAD profiles were then built for each segmented ALS overstorey crown to identify the height break between overstorey crowns and sub-canopies (mid-storey and

understorey trees). The above ground ALS point clouds were then classified into two categories: overstorey vegetation and sub-canopy vegetation. The marker-control watershed segmentation was then used to segment the overstorey crowns and sub-canopy crowns separately for these two point clouds. The result of detected sub-canopy trees from the Hovermap datasets were used as a reference to select the suitable set of parameters for the marker-control watershed segmentation to segment the subcanopy crowns in the ALS dataset.

Plot-level analyses

As mentioned above, there are now numerous lidar software packages available for processing and analysing lidar data (e.g., LAStools, FSCT, lidR). The plot-level and broader scale analyses presented below applied various combinations of these software packages.

Voxel size

The vertical distribution of points for a particular location (e.g., a plot) is commonly used to produce different metrics that represent forest structure. ALS has a reasonably uniform pulse density, however the same cannot be said for MLS, where pulse density is impacted by the distance between the object and scanner, and the walking speed of the operator. To account for this non-uniformity, the point cloud can be normalised using voxels. The process involves placing a 3D grid of specified dimensions over the point-cloud and recording the presence/absence of points within each voxel (cube). Voxel size is important to correctly represent the actual foliage density at a given height. If the voxel size is too small, there will be too many internal gaps between foliage, and it will underestimate the real foliage density. On the other hand, if the voxel size is too big, the true foliage density will be overestimated.

A range of voxel sizes were tested to assess their impact on the vertical profile and common lidar metrics. A 10 cm voxel size was selected for further analysis and is used in most of the remaining Hovermap analysis in this section. In the voxelisation process used here, each voxel that contains at least one point was recorded as a single point in the centre of the voxel. The number of points in each voxel was also recorded (replacing the intensity value). Giving equal weight to a voxel containing a single point to a voxel containing many points may be problematic. To test this effect, voxels with low numbers were progressively filtered from the dataset.

Plot-level vertical distribution vegetation patterns using Hovermap data

Due to the much higher and irregular point densities from MLS data compared to ALS data, the traditional approach (e.g., Bouvier *et al.* 2015) to determining leaf area density across various vegetation layers is not practical. Therefore, approaches to obtaining uniform distribution patterns of Hovermap data, such as voxelisation (as described above) and filtering last returns only were examined for comparing LAD profiles. Two approaches were considered, one based on the relative returns after voxelisation and a second which applied a new canopy profile model to characterise the vertical structure. For the later approach, instead of using gap fraction at a given height (z), the approach used the projection coverage of point clouds to represent the foliage density for that height level (z), called the foliage coverage profile (FCP). The projection coverage of points at given height (z) can be adjusted by the voxel size of points.

Plot-level lidar metrics

Many lidar metrics are based on the vertical height distribution of points for the whole plot. While numerous metrics have been proposed, many are highly correlated and therefore somewhat redundant. In general, metrics describing height, variation in height and vegetation cover will support a range of applications (White *et al.* 2013). Metrics used here included top height, mean height, standard deviation, coefficient of variation (CV), skewness and kurtosis. CV summarises the relative variation of the height distribution and as a measure of crown density, higher CV values indicate sparse, open canopies and low CV values dense, closed canopies. Haywood & Stone (2011) interpreted that positive skewness values were associated with sparse canopies and negative values with closed canopies when using ALS data to estimate structural attributes of mountain ash (*Eucalyptus regnans*) forests in Victoria.

Evaluation and comparison of vertical profiles for Hovermap and ALS data

As mentioned above, two approaches were undertaken for this evaluation, the first examined profiles based on relative counts of points for the ALS data and voxels for the MLS data and the second compared leaf area density and foliage cover profiles.

In the first approach, in addition to the six ‘fully monitored’ plots, field and Hovermap data from an additional five plots located and assessed on the private properties were also included. The data were processed by Interpine Innovation into height normalized 3D point clouds for circular plots with a 25 m radius. The same plot areas were extracted from the ALS capture for comparison between data sources.

To increase the sample size to 44, four non-overlapping subplots were created in each larger plot to further explore the relationships between the ALS and Hovermap data. In a statistical sense, this process may be considered pseudo-replication, due to the spatial autocorrelation between subplots. However, it was only used here to aid interpretation in the comparison of the lidar metrics. Due to a rotational shift, the subplots were aligned manually using the canopy height models (CHM) to ensure that they covered the same area (Figure 7).

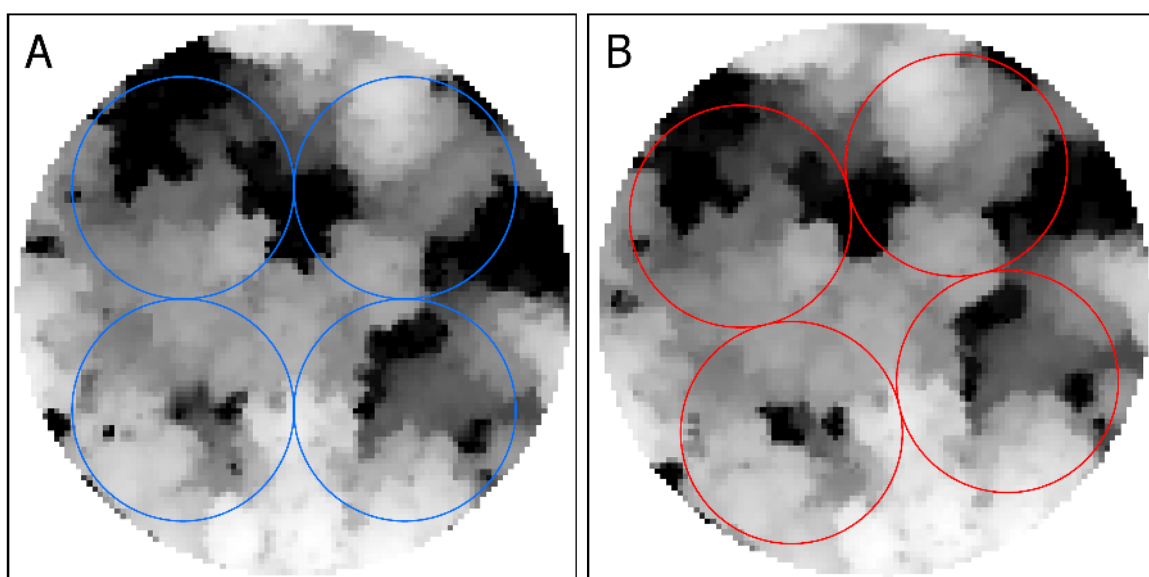


Figure 7. Example of canopy height models for the ALS (A) and Hovermap (B) data for a sample plot, showing the location of four subplots

A number of standard lidar metrics were extracted from both the ALS data and the Hovermap 10cm voxel data. The metrics used here included: Height at the 95th percentile (p95), Average height (avg), Density (dns; number of points above 2m divided by all points), Coefficient of variation (cv), Skewness (ske) and Kurtosis (kur). All metrics except for density use a height cut-off of 2 m. Although canopy cover is typically used for ALS data, its calculation uses 1st returns, which is not compatible with the Hovermap data in this context.

Comparison of ALS and MLS cover estimates

A comparison of percent cover in each cover class (as defined in the field-based manual) was undertaken, where lower storey is > 1.3 m and less than 2 m, mid storey is > 2 m and < 10 m, and upper storey is > 10 m. Emergent canopy (treetops sticking out above the canopy) was combined with upper storey for this exercise. It is difficult to directly compare cover between the sensors, due to the different point densities. The method employed here was to filter the points based on height class and then create a canopy height model (CHM) for each class using a 25 cm pixel size. The CHM algorithm used was a simple point to raster conversion, where the highest point in each raster cell is used. Cover was then calculated for each height class as the percentage of pixels in the plot with any cover. A 0.1 ha plot (radius 17.84 m) was used here as per the field data.

Derivation of fuel hazard metrics and fuel connectivity using Hovermap data

For each plot, the height normalised Hovermap point clouds were translated into a 3D voxel space, using a voxel size of 4 cm. This was done to normalise the point density across each plot. A voxel was considered filled when it contained at least one point. The resultant output was a 3D model that indicated the presence and absence of vegetation elements across the plot. Mean vegetation height and cover was estimated for each strata layer from the reclassified Hovermap point clouds. Using the voxel space models, the mean height was calculated as the average surface height of the top layer of each column within each strata layer. Percent cover was then determined as the number of voxel columns within each strata layer that had at least one filled voxel.

A vertical layer pouring algorithm (Hillman *et al.* 2021) was then used to identify the connection between different vegetation layers, which considers any element that is directly adjacent or overlapping with a higher strata layer to be a part of that layer. Each voxel is assigned a unique identifier depending on its connectiveness to neighbouring voxels, both horizontally and vertically and the procedure repeated for each voxel layer continuing downwards. Each voxel is then assigned to a strata class based on the Overall fuel hazard assessment guide (OFHAG) height thresholds. The strata layers used in this assessment were near-surface (< 0.6 above ground height (AGH)), elevated (< 0.6 m – 3 m AGH), sub-canopy (3 m – 5 m AGH) and canopy (> 5 m AGH) (OFHAG; Victorian DS&E, 2010).

Due to the noise present within the Hovermap point clouds and the difficulty discerning points representing the ground surface layer and surface level vegetation, only the near surface and elevated fuel layers derived from the Hovermap point clouds were assessed in comparison to those acquired using visual assessment practices.

Evaluation of GEDI data for characterising forest structure changes following wildfire

GEDI Version 2 data for each of the study sites were downloaded. The ISS has an irregular orbit, so the GEDI samples are also irregular in space and time. Figure 8 indicates GEDI samples available over one of the ALS transects. Due to limited actual GEDI samples that coincided with the ALS captures, the decision was made to simulate GEDI observations using the GEDI simulator (Hancock *et al.* 2019). The simulator also allows for two time-steps of the same footprint location to be directly compared (one of which could be a real GEDI observation).

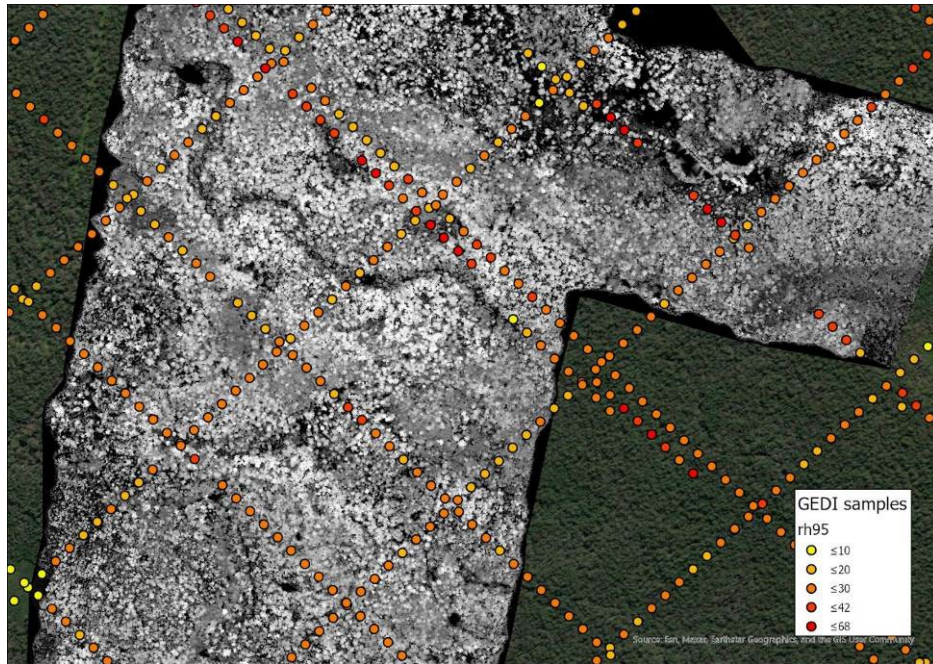


Figure 8. GEDI footprints over a canopy height model of one of the ALS transects

ALS data were available over the study sites for two points in time: April/May 2020 and April/May 2021. Thus, the ALS was captured after the 2019/2020 wildfires, providing two points in time to explore short-term forest recovery. Virtual GEDI observations were simulated from the ALS for all the real GEDI footprint locations. This resulted in two sets of simulated RH observations for every footprint location: one from 2020, and one from 2021. Forest recovery was then assessed as change across all relative height (RH) metrics between 2020 and 2021.

The aim was to investigate structural recovery shortly after fire and then one year later. The simulated datasets were therefore filtered only to areas that intersected with the NSW fire history records. In addition, non-forest observations were discarded, using the forest type map from Australia's State of the Forests Report 2018. Following this the simulated footprints were intersected with the Fire Extent and Severity Mapping (FESM) product (<https://datasets.seed.nsw.gov.au/dataset/fire-extent-and-severity-mapping-fesm>) to extract fire severity information. The FESM outputs, based on modelled satellite data, broadly matched the visual plot assessment of fire severity (plot 18553_10_a – low, plots 1384_FI1_hc & 25703-02_bc – Moderate and plot 20736_FI1_a – High). Due to some areas

within the fire history layer being unburnt (according to FESM), some unburnt footprints remained. The final number of samples in each class is shown in Table 3.

Table 3. Number of simulated GEDI observations in each fire severity class

Fire Severity	Number of samples
Unburnt	272
Low	180
Moderate	204
High	294
Extreme	66
Total	1016

Project data management

A secure directory channel in the NSW DPI Microsoft TEAMS system was established, with all project research collaborators given access. All the project datasets and related reports were uploaded into this channel and were manually checked for obvious errors.

Results

A detailed description of the six field plots is provided in Tables 1 and 4 and Figure 3 and illustrate that although only six plots were assessed in this scoping study, they presented a range of multi-layered structures. In particular, the plots that had been burnt during the 2019 bushfires in eastern NSW (Plots 1384_FI1_hc and 25703_02_FI1_bc with moderate fire damage and, Plot 20736_FI1_a with severe fire damage).

Tree-level analyses

Manual comparison of field and Hovermap tree-level measurements

The detailed comparison of matched trees obtained from the field (distance and bearing) measurements and from the Hovermap tree data from Interpine Innovation for three plots (01384_FI1_hc, 26412_FI1_ec and 26739_1a) revealed that while there was a close match for the larger trees (DBH > 300 mm) in all three plots, significantly more smaller diameter trees were identified in the Hovermap data. Figure 9 illustrates the matched trees for Plot 26412_FI1_ec. This plot was established on a steep slope (23 degrees), had not been recently burnt but contained moderate amounts of understorey vegetation (Figure 3c, Tables 1 and 4).

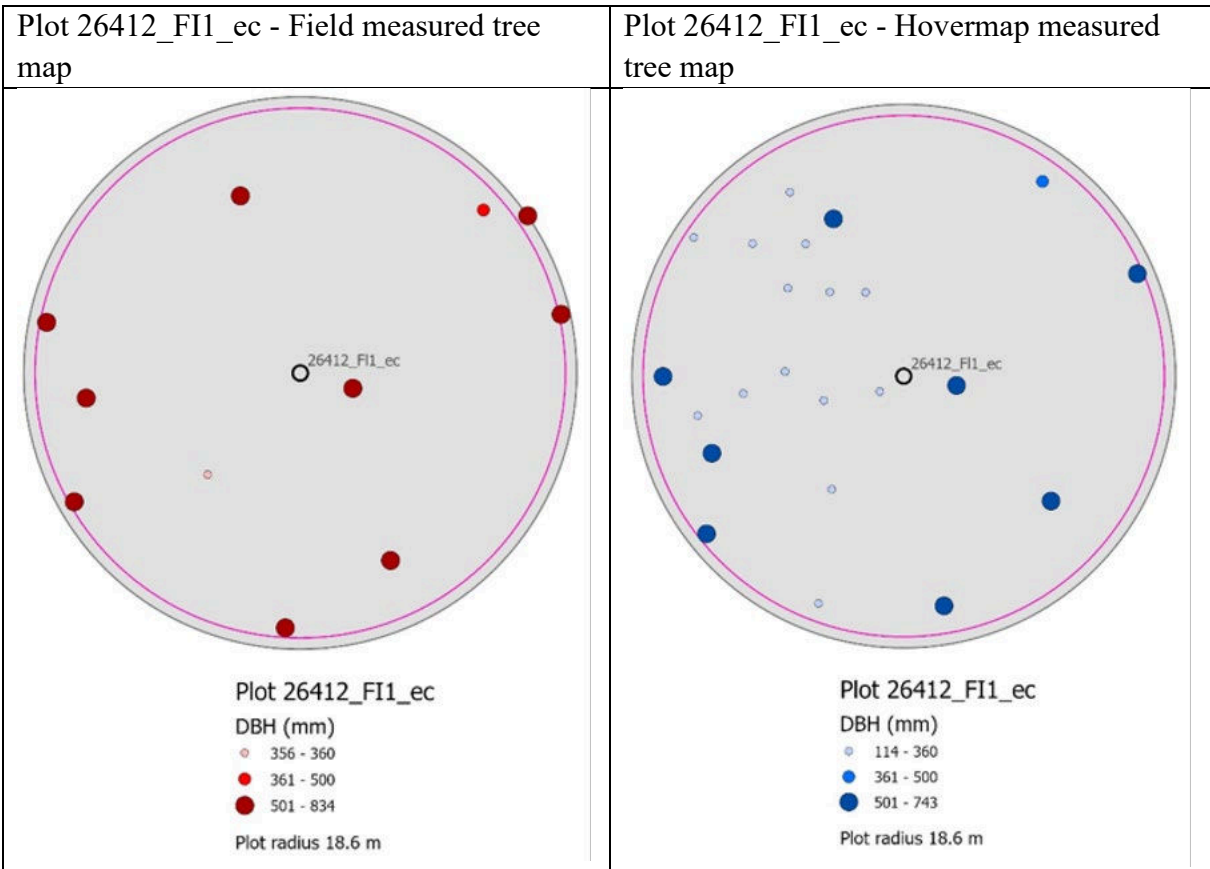


Figure 9. Comparison of manually matched trees located from the field and Hovermap datasets for plot 26412_FI1_ec

The difference in DBH measurements between the inventory field and Hovermap datasets for a subset of carefully matched trees ranged from 3 mm to 91 mm (absolute mean = 15.45 mm;

S.D. = 19.13 mm; S.E. = 4.28 mm), while the differences in tree height ranged from 0.2 m to 2.67 m (absolute mean = 0.709 m; S.D. = 0.838; S.E. = 0.187 m) (Table 4). There appeared no obvious trend in bias for the difference for these two tree parameters.

Table 4. Comparison of tree DBH and heights for a subset of larger trees located in the field and Hovermap datasets for plots 01384FI1_hc and 26412FI1_ec

Plot ID	Field tree ID	Hovermap tree ID	Field DBH (mm)	Hovermap DBH (mm)	Δ Hovermap DBH – field DBH (mm)	Field tree Ht. (m)	Δ Hovermap Ht. - field Ht. (m)*
01384_FI1_hc	11	14	485	491	6	21.8	-1.32
01384_FI1_hc	13	19	102	119	17	10.1	-0.52
01384_FI1_hc	12	21	113	135	22	10.0	-0.24
01384_FI1_hc	19	25	285	289	4	21.5	-0.37
01384_FI1_hc	22	27	684	661	-23	21.8	-1.94
01384_FI1_hc	25	32	229	216	-13	18.0	-0.02
01384_FI1_hc	27	36	432	428	-4	14.0	0.76
01384_FI1_hc	30	38	620	602	-18	29.3	-2.19
01384_FI1_hc	40	44	122	116	-6	11.1	-0.11
01384_FI1_hc	43	63	291	294	3	21.2	-2.05
26412_FI1_ec	21	3	451	441	-10	19.7	-0.44
26412_FI1_ec	22	4	643	631	-12	42.1	-2.67
26412_FI1_ec	1	5	834	743	-91	34.6	0.073
26412_FI1_ec	2	7	571	561	-10	25.7	0.004
26412_FI1_ec	3	8	543	539	-4	22.0	0.37
26412_FI1_ec	5	11	356	337	-19	19.0	0.32
26412_FI1_ec	6	12	718	729	11	30.0	-0.05
26412_FI1_ec	7	13	518	510	-8	18.7	0.29
26412_FI1_ec	13	15	669	666	-3	32.2	0.44
26412_FI1_ec	18	27	686	661	-25	32.5	0.003

*Comparisons based on the Hovermap tree location

Evaluation of the FSCT to extract tree-level attributes from Hovermap data

The Hovermap data of plot I8553_I0_a was used to test the processing efficiency of the last returns only dataset (MLS_{r1}) compared with the outputs of all returns (MLS_a). With the same set of parameters in FSCT, the processing time of MLS_a was 441.8 minutes while the time of MLS_{r1} was 166.9 minutes. The last returns reduced the processing time by 60%. The number of detected trees for MLS_a was 1785 stems per ha, while the number detected trees of MLS_{r1} was 855 stems per ha. Compared to the field results (Table 7), the MLS_a data had a significantly higher stem count estimation while the MLS_{r1} data provided a stem count per ha compatible with the Interpine processed data. Both the FSCT and Interpine analysis produced higher stem counts per ha than was recorded by the field-crew, but this is understandable as only trees with DBH > 10 cm were measured by the inventory crew, small trees with DBH < 10 cm were only measured in the inner subplot having a radius of 3.99 m and analysed separately. A detailed examination of the FSCT stem cylinder maps revealed that most of the non-detected stems by the MLS_{r1} data are for trees with DBH < 10 cm (Figure 10). Figure 11 presents a frequency histogram of the DBH size classes apparently missed by the MLS_{r1} when compared by the MLS_a data.

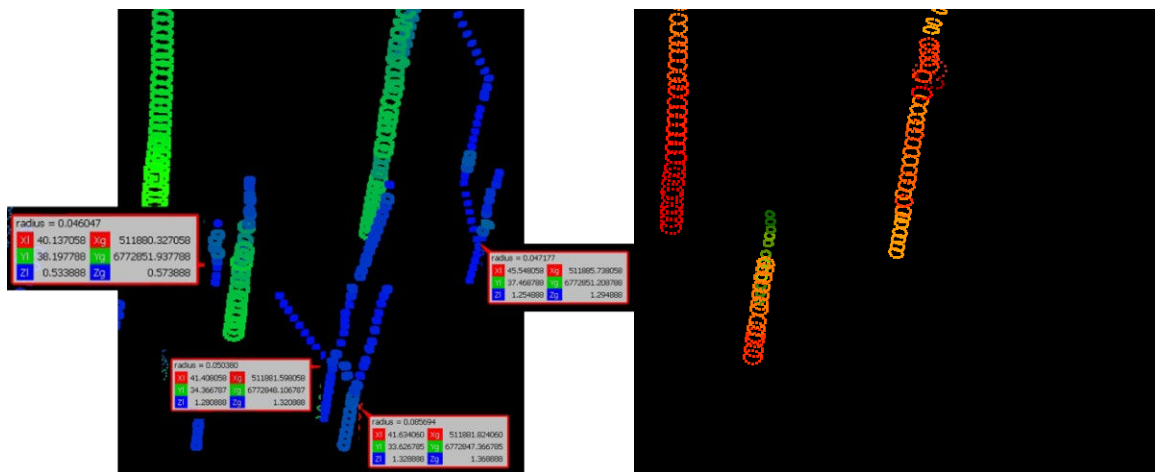


Figure 10. Illustrating the detection of stem cylinders in the MLS_a (green and blue stems) and the MLS_{r1} data (red stems aligned with the same green stems but smaller blue stems missing).

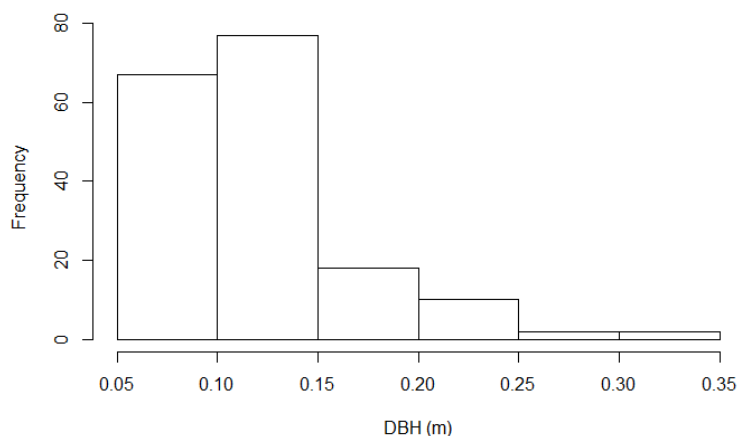


Figure 11. A histogram of DBH size classes of stems identified as missing in the MLS_{r1} data

Comparison of DBH and tree height between field measurements and FSCT outputs

DBH values were compared using the field plot data and the stem maps produced from first returns (MLS_{r1}) in the FSCT. Individual trees were matched for plots 1384_FI1_hc and 26412_FI1_ec (Figures 12a and 12b). For these two plots, the FSCT accurately estimated the DBH of individual trees. The R^2 of plot 1384_FI1_hc is 0.754 and in plot 26412_FI1_ec it is 0.991 (Figure 12a). Figure 12b combines both datasets and also provides a 1:1 line.

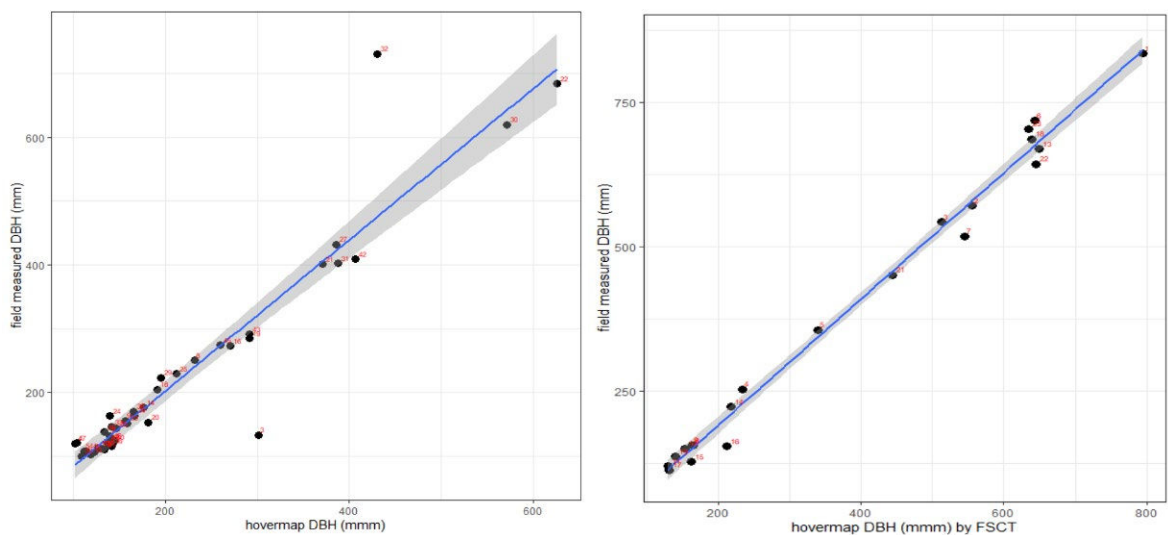


Figure 12a. Tree-level comparison of DBH between the field measurements and the FSCT outputs of the MLS_{FI} datasets for plots 1384_FI1_hc (left) and plot 26412_FI1_ec (right). Fitted regression lines shown in blue.

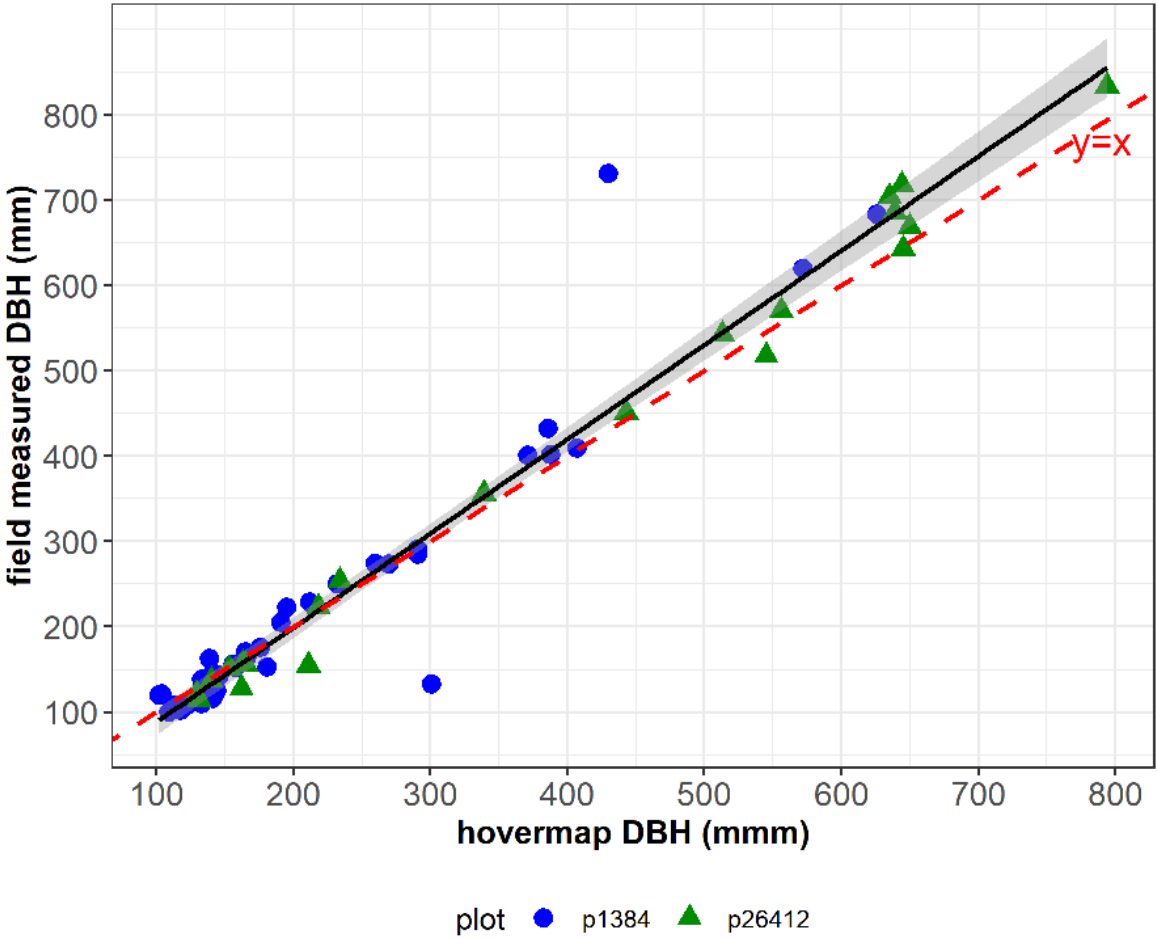


Figure 12b. Both graphs presented in Figure 12a combined, with a fitted regression line in black and 1:1 line in red.

There was, however, a much poorer correspondence when this exercise was repeated for tree height. Examination of the MLS_{r1} data indicated that the FSCT failed to accurately extract tree heights for the sub-canopy trees. This is examined further using tree-level PAD profiles.

Height estimates using the tree level PAD profiles

The tree-level PAD profiles are illustrated in Figure 13 and show the relative plant area density of the MLS and how it changes with vertical canopy height (z values). For sub-canopy trees over-topped by relatively few upper-canopy tree crowns (Figure 13 a, b and c), there is a large vegetation density gap between the highest point clouds and the sub-canopy point clouds. The relative density at the height break for this type of sub-canopy tree is close to zero. Where sub-canopy trees are hidden under dense overstorey there is no clear height break or zero vegetation density layer of the foliage and stem PAD (PAD_{fs}), but a height break can be identified by the stem only point cloud density profile (PAD_s) (Figure 13d). With the adjustments of sub-canopy height using the PADs and by comparing with field-measured tree height, the tree height of MLS_{r1} datasets were successfully extracted (Figure 14 a & b). The R^2 of tree height was notably improved – in plot 1384_FI1_hc it was 0.913 and in plot 26412 FI1_ec it was 0.798.

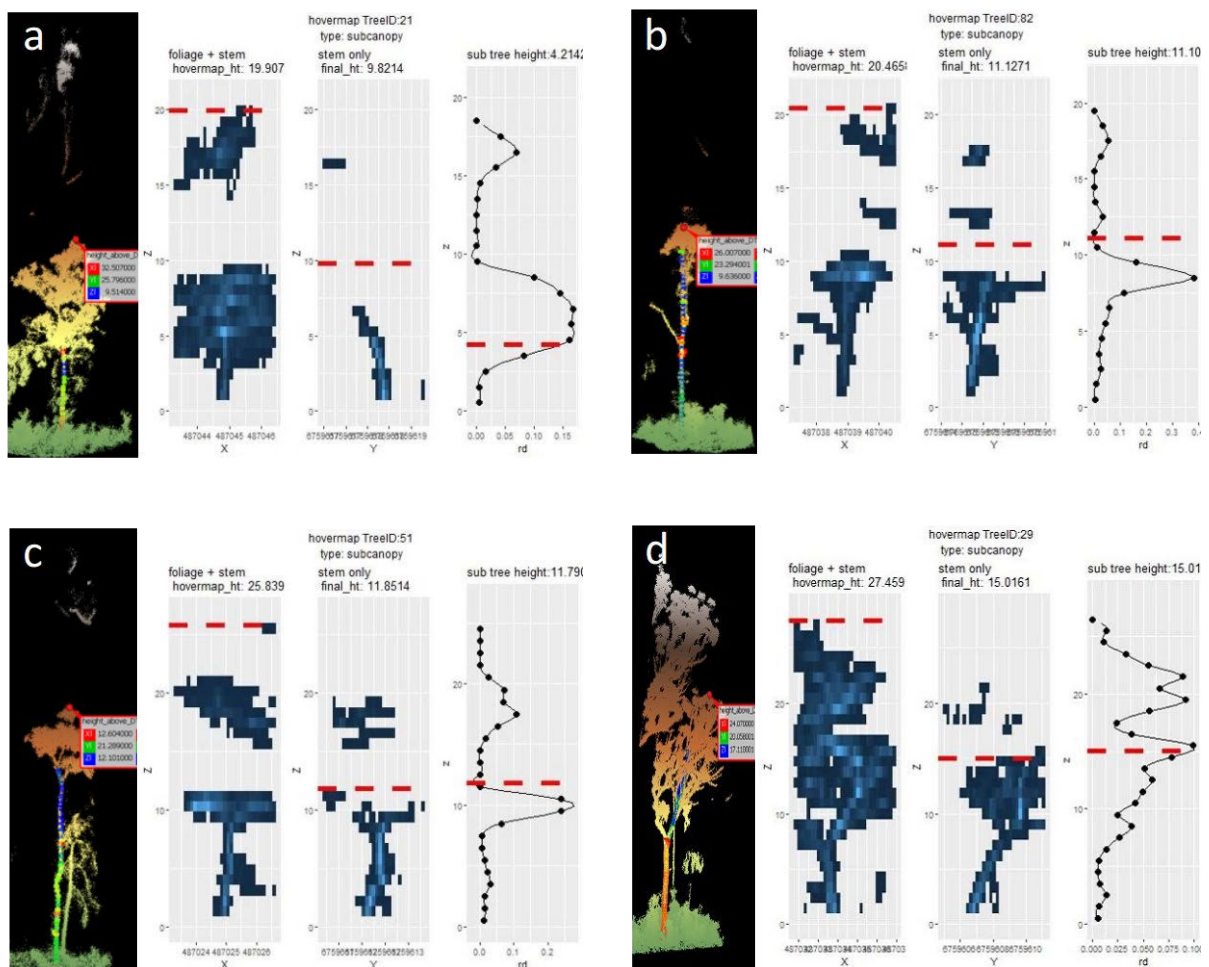


Figure 13. Examples of estimates of tree height for sub-canopy trees using tree-level Plant Area Density (PAD) profiles. The y-axis represents tree height (Z). In panel 2 of each group,

voxel densities are shown in the X direction (foliage + stem), while in panel 3, they are in the Y direction (stem only). Panel 4 shows the relative density (rd) of voxels across height levels.

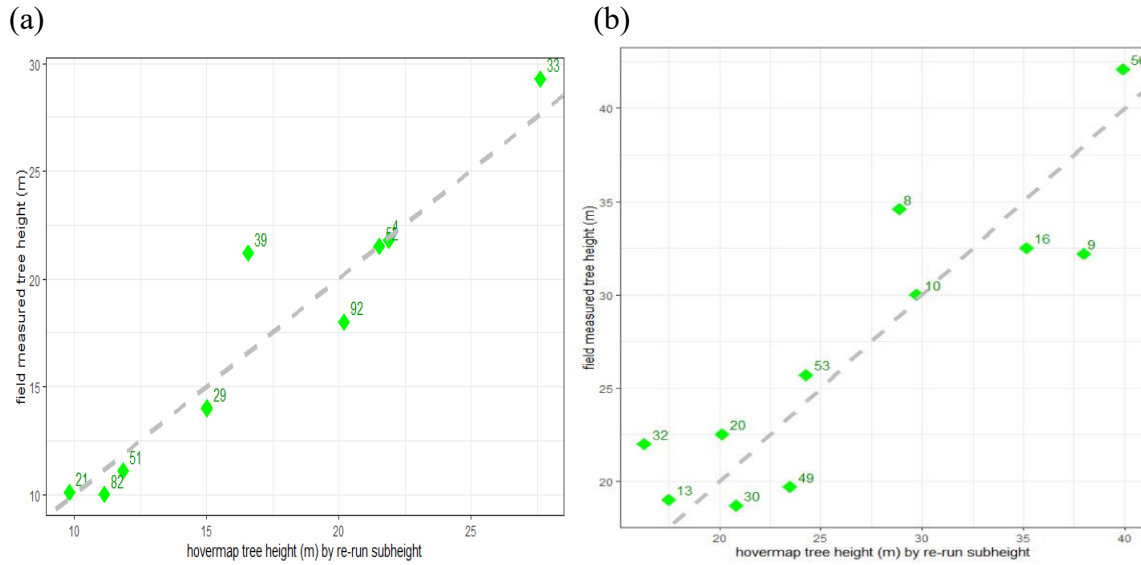


Figure 14. Comparison of tree heights between field measurements and detected sub-canopy height by PADs for plot 1384_FI1_hc (a) and plot 26412 FI1_ec (b)

Standing stag or dead-top tree detections using MLS data

By comparing the tree-level plant area density profile between foliage only (PAD_f) and stem only (PAD_s) point clouds, we found that standing stag or dead-top trees could be identified. For the PAD_s of stag trees, there is no clear height break in PAD_s but a clear height break in PAD_f (Figure 15). Meanwhile, as a stag, the total plant area density above half of the tree height of stems is higher than the density of foliage. Whereas in the types of live trees (live overstorey and sub-canopy tree), the top layer plant area density of stems is always lower than the density of foliage. Even for a sub-canopy stag (Figure 15d), after accurately identifying the tree height, based on the PAD of the top foliage points being lower than stems, we could identify this sub-canopy stag.

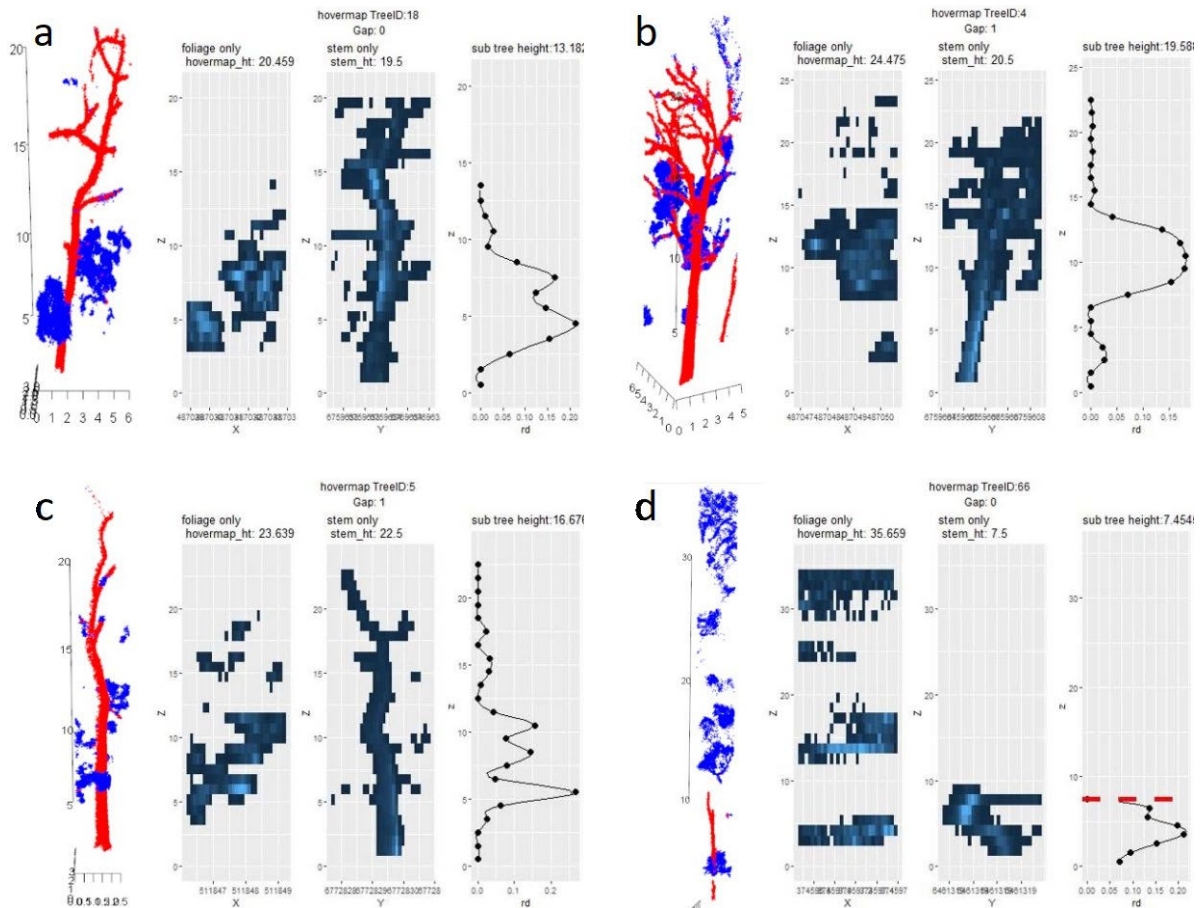


Figure 15. Examples of Plant Area Density profiles for stags in plot 1384_FI1_hc (a and b), plot 18553_I0_a (c), and plot 26412_FI1_ec (d). The y-axis represents tree height (Z). In panel 2 of each group, voxel densities are shown in the X direction (foliage + stem), while in panel 3, they are in the Y direction (stem only). Panel 4 shows the relative density (rd) of voxels across height levels.

Summary of crown types extracted from the Hovermap data from the 3 plots

As shown in Table 5, the highest stem density of stags and lowest stem density of sub-canopy trees is in plot 1384_FI1_hc. The proportion of sub-canopies in both plot I8553_I0_a and plot 26412_FI1_ec are very similar, around 77-78%. The tree size in both overstorey and sub-canopy trees in plot 26412_FI1_ec are bigger than the trees in plot I8553_I0_a and plot 1384_FI1_hc. While a direct comparison of the field data in Table 6 with the results in Table 5 is not possible, the relative ranking of the tree attributes corresponds very closely, including the MLS derived information on the dead stag trees.

Table 5. The number of trees per plot, the average DBH (m) and the average tree height (m) of each crown types, extracted from Hovermap data

Plot ID	all			overstorey			sub-canopy			stag or dead top		
	Trees /plot	DBH (m)	height (m)	Trees /plot	DBH (m)	height (m)	Trees /plot	DBH (m)	height (m)	Trees /plot	DBH (m)	height (m)
01384_FI1_hc	83	0.213	14.5	27	0.290	18.6	47	0.152	11.3	9	0.298	19.1
18553_I0_a	173	0.195	14.8	35	0.252	19.7	134	0.176	13.4	2	0.524	24.5
26412_FI1_cc	60	0.311	17.5	12	0.459	27.0	47	0.265	15.1	1	0.713	16.0

Detection of tree-level subcanopy vegetation in ALS data

The marker-control watershed segmentation algorithm was applied to identify individual overstorey crowns in the ALS data. Repeating the approach used with the Hovermap data, the height break between the overstorey crowns and sub-canopies was also successfully identified from the ALS PADs (Figure 16 a & b). Based on the marker-control watershed segmentation applied separately to the overstorey and sub-canopy point clouds, a total of 63 overstorey crowns and 182 sub-canopy trees were detected from the ALS data for plot 18553_I0_a (Figure 17 a & b).

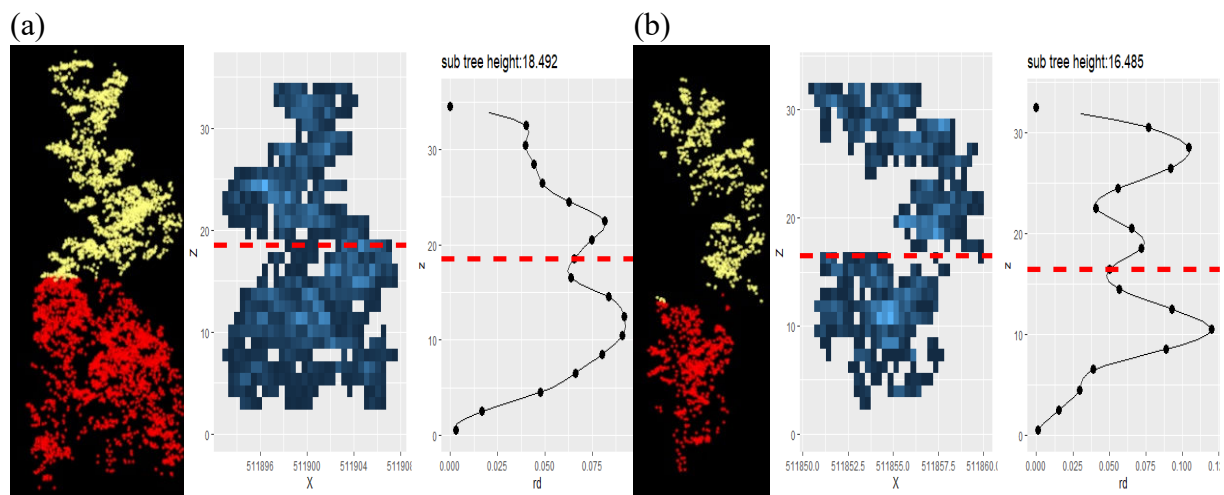


Figure 16. Examples of PAD profiles for ALS individual crowns and identified height breaks between overstorey and sub-canopy height.

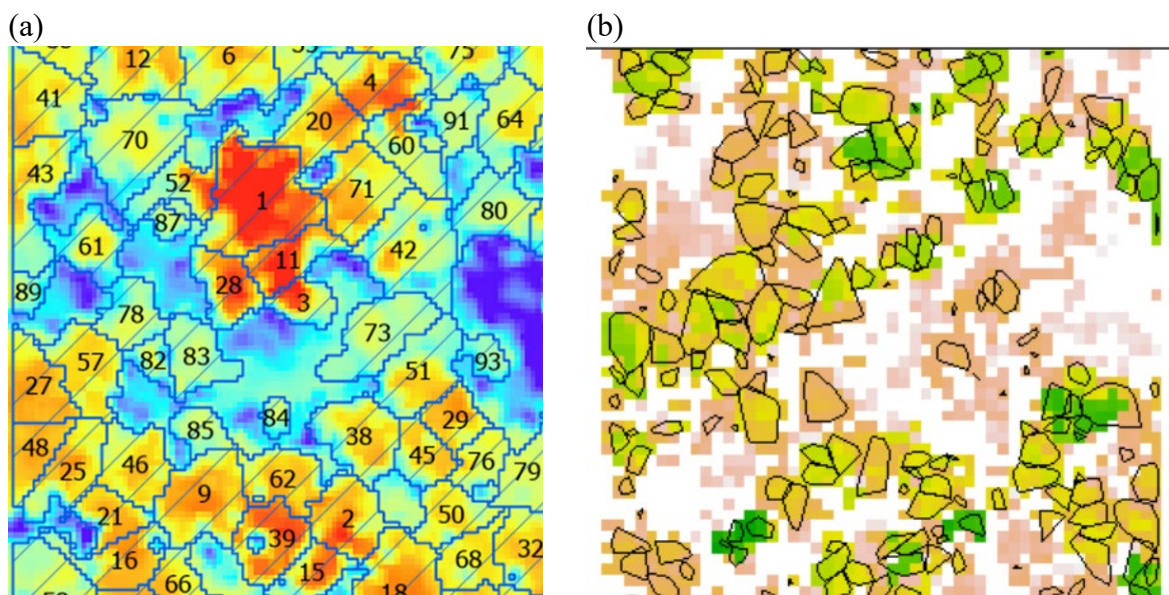


Figure 17. The canopy height model (CHM) and segmented individual crown map of (a) overstorey vegetation and (b) sub-canopy vegetation from the ALS data for plot 18553_I0_a

Plot-level analyses

Summary of field measurements presented at a plot level or per hectare basis

While all six ‘fully monitored’ plots presented complex vegetation structure they were different in terms of their structure and composition (Table 6). Plot 25703-02_FI1_bc had the largest BA and the highest ‘emergent canopy cover’ score (8%), with some of the tree crowns scorched from the 2019-2020 bushfire. This plot also had dense regrowth, likely due to fire recovery and its location in a riparian area (Figure 3d). Not surprisingly, the most severely burnt plot, Plot 20736_FI1_a, had the lowest BA and lowest canopy cover estimates, with the remaining trees receiving low crown health scores and presenting dead branches and epicormic growth. Notably, this plot was burnt following a selective harvesting event. Dense regrowth was also present in this plot (Figure 3c). Table 6 also presents plot averages of the visual estimates at each of the five-point locations, however, considerable within plot variation was observed.

Table 6. Summary of plot structure and condition of the six ‘fully monitored’ plots

Plot ID	1384_FI1_hc	18553_I0_a	20736_FI1_a	25703-02_FI1_bc	26412_FI1_ec	26739_I0_a
Slope adjusted field plot area (ha)	0.101	0.100	0.102	0.100	0.109	0.110
Hovermap plot area (ha)	0.1	0.1	0.1	0.1	0.1	0.1
Live stems/ha	317	680	159	350	212	299
Dead stems/ha (% dead to live stems)	149 (47%)	20 (3%)	217 (136%)	90 (26%)	0 (0%)	0 (0%)
Average DBH (mm)	218	213	238	282	317	287
Basal area - live trees DBH > 100 mm (m ² /ha)	23.6	22.8	8.5	42.8	32.9	28.7
Average height (m) - Healthy trees*	17.9	21.1	25.9	27.6	21.6	29.1
BA (m ² /ha) of dead trees	8.14	0	8.53	1.89	1.47	0
Overall tree crown ‘healthiness’ score**	13.5	19.6	8.3	14.3	19.0	22.3
Emergent canopy cover (%)***	0	2	0	8	0	0
Upper storey canopy cover (%)	19	14	13	23	16	28
Mid-storey canopy cover (%)	9	33	6	7	17	12
Lower storey canopy cover (%)	5	1	4	13	4	8
Canopy cover >1.3 m using ‘% cover’ App.	33	50	23	51	36	48

*7-12 trees with DBH > 10 cm

**Crown healthiness score: 25 = very vigorous health crown; 5 = crown with obvious dieback

***Averaged canopy cover estimates as a % for Lower storey > 1.3 m and < 2 m, Mid-storey > 2 m and < 10 m, Upper storey > 10 m, Emergent trees with crowns above the Upper storey. Plot canopy cover = average visual estimates obtained from the 4 cardinal points and plot centre. Percent canopy cover was based on photo area cover by plant material using the application ‘% Cover’

Overall, there was a positive (right-sided) skewed distribution for stem size distribution across all six plots. Plot 18553_I0_a had the highest stem density, with most stems in the smaller diameter classes (Figure 18). Examination of the percentage of dead trees per plot reflect the

observed fire severity following the 2019–20 bushfires, with plot 20737_FI1_a the most severely burnt plot, plots 1384_FI1_hc and 25703-02_FI1_bc assessed as moderately burnt and plot 18553_10_a lightly burnt (Table 1). Plot 20736_FI1_a was burnt following a selective harvesting event. In addition, the majority of dead trees in the fire impacted plots are in the diameter classes of 100-200 mm and 200-300 mm. Many of the remaining trees in the fire-affected plots had low crown health scores presenting dead branches and epicormic growth (Table 6).

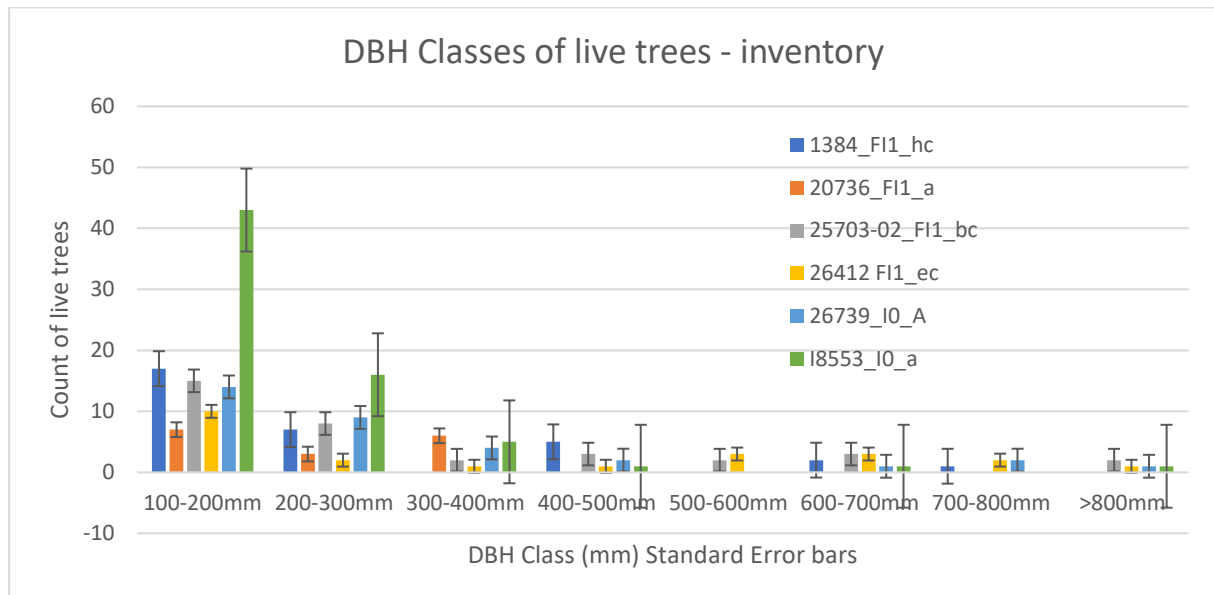


Figure 18. DBH classes of live trees

Comparison of inventory stem counts/ha and basal area with Hovermap derived estimates (Interpine Innovation)

As was shown in the analysis using the FSCT, the differences between the inventory and Hovermap data were largest for total stem counts/ha, ranging from 8.5% to 33% while the differences for BA ranged from 1% to 29% (Table 7). For four of the plots, the stem counts derived from the Hovermap data were greater than from the field inventory data. The tree-level examination indicates that the stem count errors are mostly associated with smaller stems, hence would have a lesser effect on overall BA estimates. The field inventory stem count, however, was higher than obtained from the Hovermap data for the most severely burnt plot 25703-02_bc and 26739_10_a, which had recently been selectively harvested. Both of these plots had dense undergrowth that would have resulted in stem occlusion, as well as making it difficult to walk at a consistent pace along the Hovermap survey pathway. A notable difference between the field inventory and Interpine’s Hovermap tree-level workflow is that the later does not distinguish between live and dead stems.

Table 7. Comparison of the number of stems and basal area acquired from the field and Hovermap assessments (from Interpine Innovation) for trees > 100mm DBH

Plot ID	1384_FI1_hc	18553_I0_a	20736_FI1_a	25703-02_FI1_bc	26412_FI1_ec	26739_I0_a
Inventory live stems/ha	317	680	158	350	212	680
Inventory dead stems/ha	149	0	217	90	0	0
Inventory total stems/ha	466	680	375	440	212	680
Hovermap stems/ha	520	880	500	370	230	600
Inventory live BA (m ² /ha)	23.6	36.6	8.5	40.9	33.0	28.7
Inventory dead BA (m ² /ha)	2.6	0.0	10.4	1.9	0.0	0.0
Inventory total BA (m ² /ha)	26.2	36.6	18.9	42.8	33.0	28.7
Hovermap BA (m ² /ha)	26.8	37.2	16.4	33.1	31.3	34.0

The results above highlight the difficulty in determining the source and type of errors associated with stem counts, especially for trees with DBH < 30 cm. Both omission (e.g., due to occlusion) and commission errors may have occurred for both the on-ground inventory and MLS data analysis. In the presence of dense understorey, it cannot be assumed that the manual survey was error free. To determine if ‘double counting’ may have occurred due to sensor data (SLAM) slippage or drift, the Hovermap point clouds from two plots (18553_I0_a and 20736_FI1_a) were examined in Cloud Compare. No sensor drift was detected (S. Krisanski, pers. comm.).

Comparison of the ALS and Hovermap MLS data

The point density of the Hovermap MLS is significantly greater than the ALS (Table 8). Even using 50 cm voxels, the MLS data has twice the number of points across the example plot 18553I0a. Using all Hovermap data without voxelisation results in height metrics that are substantially different than the ALS, whereas the voxelised versions are much closer. As the voxel size increases, the p50 and p95 slightly increase. As expected, the ALS indicates slightly higher values for both height metrics. The entire vertical profile for plot 18552I0a and different voxel sizes is shown in Figure 19A. This indicates that the profile using all Hovermap points is markedly different, but the profiles from each of the voxel sizes is reasonably similar. There appears to be a cross-over point at around 10 m where the ALS picks up less and the MLS more, comparatively speaking. In Figure 19B the impacts of removing voxels with low point densities is shown. This indicates that many of the higher voxels contain fewer points than the lower voxels.

Table 8. Point density and two example height metrics (p50 and p95) from the ALS data, Hovermap data and different sized voxels for plot 18553I0a

	Point density (m ²)	% >		
		2m	p50	p95
ALS	32	69.5	14.6	27.5
Hovermap	39,000	64.3	7.0	16.9
10cm voxel	2,226	81.3	10.7	23.7
20cm voxel	491	83.9	11.1	24.7
50cm voxel	63	85.8	11.3	25.3

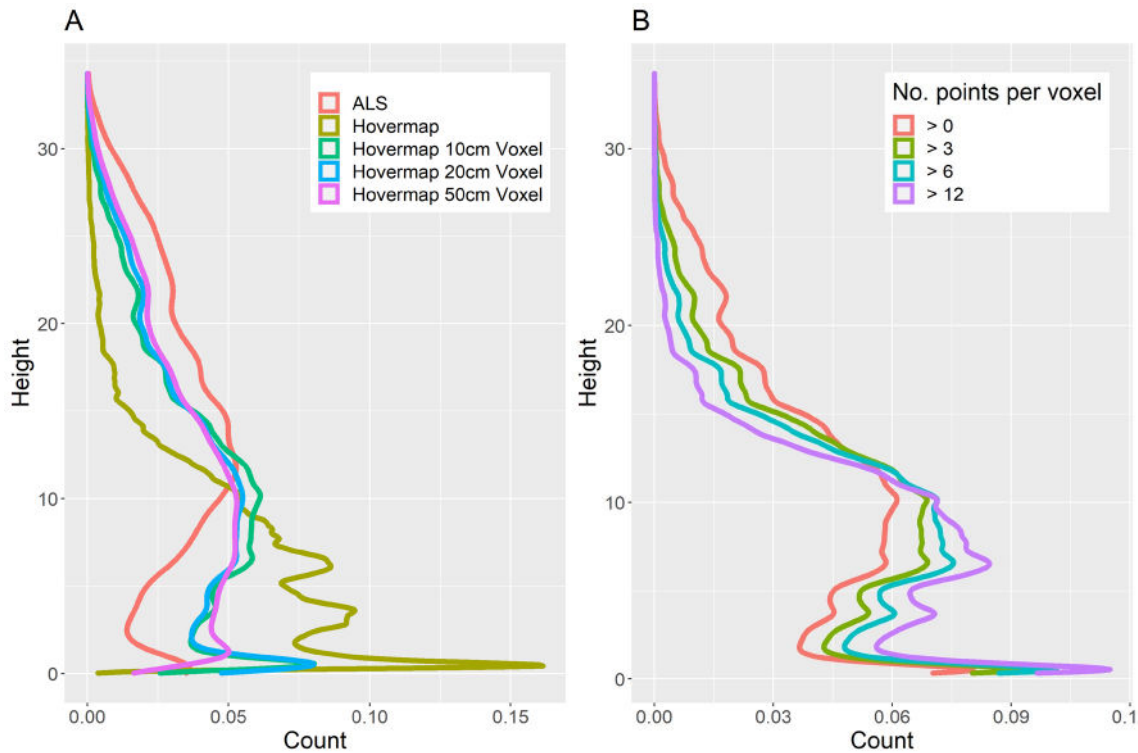


Figure 19. Vertical profiles for plot 18553I0a. In (A), different voxel sizes are compared with all Hovermap points and the ALS. In (B), voxels with a small number of points are discarded using different threshold values.

The vertical profiles for all points above 2 m are shown for three plots in Figure 20. These indicate that the ALS data favours the upper canopy, whereas the MLS favours the understory. A comparison of six common lidar metrics for both the full plots and subplots are shown in Figure 21. The three plots in Figure 20 are labelled in the charts in Figure 21. Correlations between the ALS and MLS datasets are generally high, ranging from 0.98 for p95, to 0.23 for kurtosis. However, for most metrics (all except kurtosis), there is a uniform bias. For the two height metrics (p95 and average) the ALS values are higher. The MLS data has a greater density of points and higher coefficient of variation and is also more skewed towards the ground. Kurtosis has both a low correlation and no clear bias.

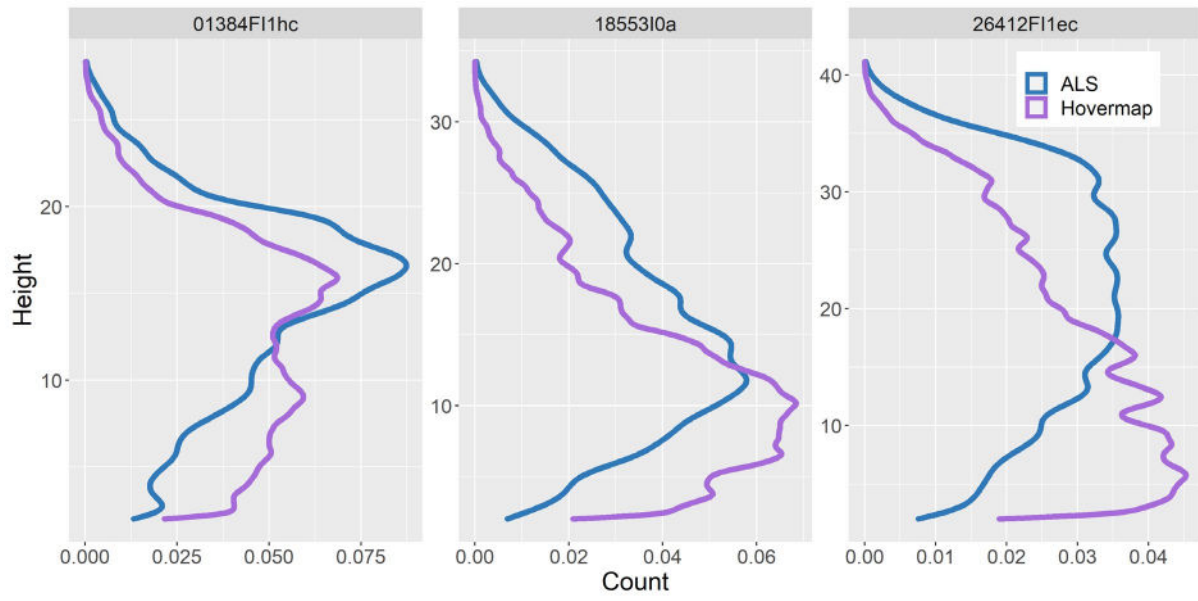


Figure 20. Vertical profiles of ALS and Hovermap 10 cm voxels for three plots for all points above 2 m in height

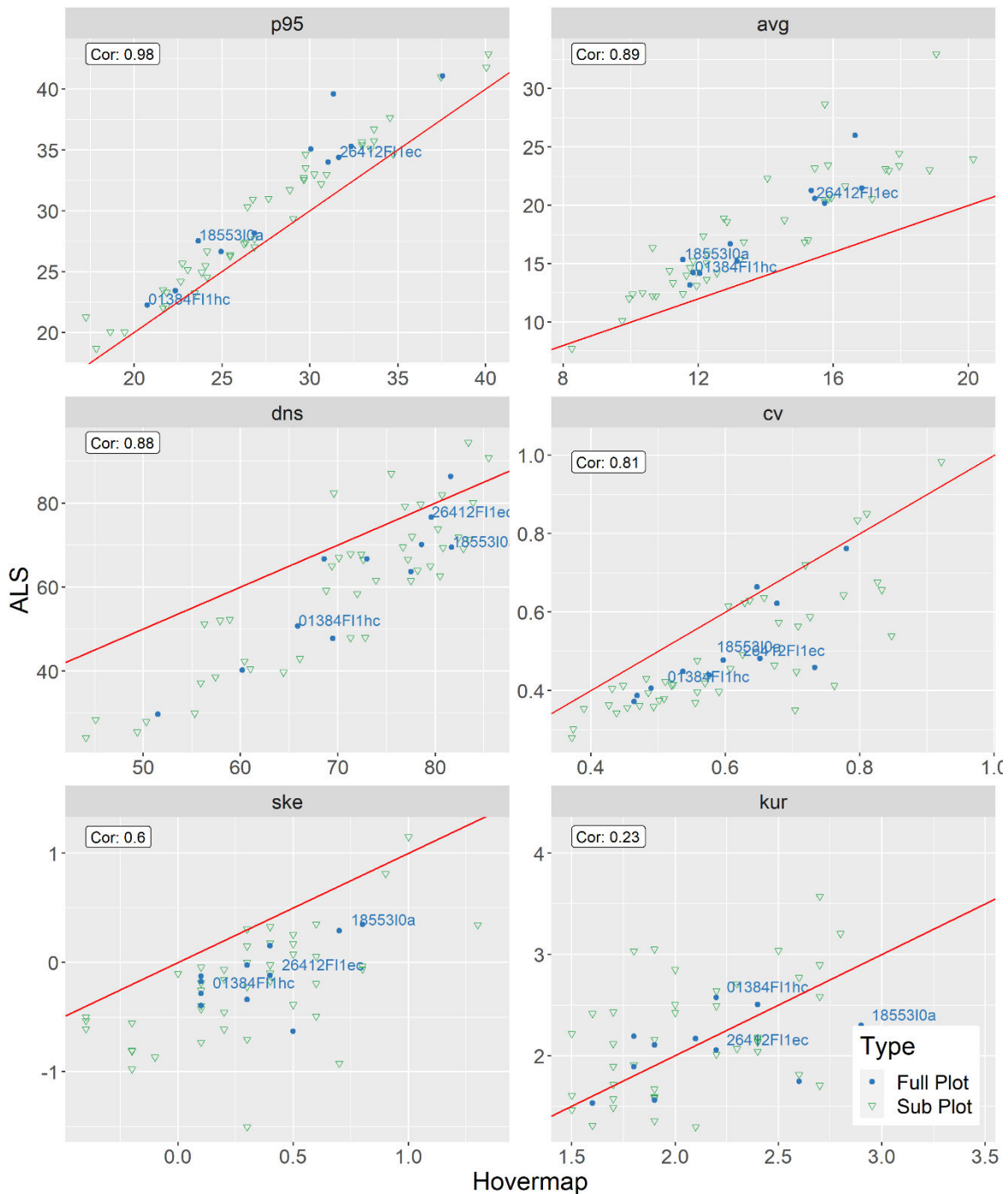


Figure 21. Comparison of common lidar metrics calculated from the ALS and Hovermap 10cm voxel products. Metrics include: Height at the 95th percentile (p95), Average height (avg), Density (dns), Coefficient of variation (cv), Skewness (ske) and Kurtosis (kur). The three plots shown in Fig. 3 are labelled. The red line is a 1:1 line. Correlation between the two datasets (subplots only) is also shown.

Table 9 provides an additional comparison of ALS and Hovermap height distribution metrics using the ALS height normalised data and the Hovermap 10 cm voxels. For all six ‘fully monitored’ plots, the p99 values were only slightly higher for the ALS data than the Hovermap data (mean = 1.46, SD = 0.624). The p99 difference was lowest for plot

20736_FI1_a, which also had the lowest estimate for total canopy cover, while the largest difference was for plot 18553_I0_a which had the highest visual estimate for the mid storey cover (Table 6). This trend of ALS data producing higher values than the Hovermap data held true for p95, p50 and average (Table 9), although the differences were greater. This trend, however, did not hold for the metrics standard deviation, coefficient of variation (cv), skewness and kurtosis. For five of the six plots, the ALS skewness values were negative (left skewed), indicating the data was dominated by the upper storey, while for the Hovermap data, all the skewness values were positive, indicating the influential presence of the understorey. The values for kurtosis were all positive but difficult to interpret. The relative differences in standard deviation were not notable except for plot 25703-02_FI1_bc (ALS 12.70 versus Hovermap 10.60), this plot also had the highest estimate in lower storey canopy cover (Table 6).

Table 9. Comparison of ALS and Hovermap height distribution metrics for the six fully monitored plots

Plot ID	1384_FI1_hc	18553_I0_a	20736_FI1_a	25703-02_FI1_bc	26412_FI1_ec	26739_I0_a
ALS metrics						
p99	26.02	30.06	28.83	42.38	37.28	36.57
p95	23.19	26.51	27.27	40.50	34.29	35.31
p50	15.69	13.90	16.32	23.43	22.96	25.62
Average	14.90	14.86	14.72	20.97	21.11	23.22
Standard deviation	5.41	6.56	9.20	12.70	9.51	9.64
Skewness	-0.30	0.37	-0.13	-0.14	-0.28	-0.64
Kurtosis	2.61	2.43	1.52	1.71	1.90	2.30
Coefficient of variation	0.36	0.44	0.62	0.62	0.45	0.42
Hovermap metrics						
P99	24.85	27.95	28.25	40.55	35.25	35.55
P95	21.65	23.35	26.15	32.45	31.85	32.65
P50	11.75	10.55	9.95	11.75	13.45	16.15
Average	12.05	11.45	11.85	14.25	15.55	16.55
Standard deviation	5.70	6.10	8.80	10.60	9.40	10.3
Skewness	0.20	0.70	0.30	0.60	0.40	0.10
Kurtosis	2.20	3.00	1.60	2.20	2.00	1.60
Coefficient of variation	0.47	0.53	0.74	0.74	0.60	0.62

A comparison of percent cover for each sensor in each of the cover categories (low 1.3–2m, mid 2–10m and upper >10m) is shown in Table 10. This indicates that cover is much higher in the MLS data, which is most likely a function of point density. In general, the ALS shows higher levels of cover in the upper canopy and lower in the mid and low classes. Two plots (20736FI1a, 2570302FI1bc) stand out as having a sparse upper canopy, with a lot of cover in the low height class in both datasets.

Table 10. Percent cover in each cover class for ALS and Hovermap 10 cm voxels

ALS				
Plot	1.3 - 2m	2 - 10m	>10m	Total > 1.3
01384FI1hc	4.1	23.0	59.1	70.9
18553I0a	1.5	24.6	58.8	70.2
20736FI1a	31.6	21.6	28.4	58.1
2570302FI1bc	17.2	30.3	50.9	78.8
26412FI1ec	2.4	25.2	74.5	82.2
26739I0a	2.9	16.8	64.8	72.1

Hovermap				
Plot	1.3 - 2m	2 - 10m	>10m	Total > 1.3
01384FI1hc	22.8	54.4	77.3	91.1
18553I0a	27.8	82.2	85.9	96.8
20736FI1a	83.6	73.8	59.7	96.2
2570302FI1bc	86.9	86.4	65.8	99.1
26412FI1ec	25.6	63.2	91.0	96.7
26739I0a	39.7	50.0	76.0	88.8

Derivation of fuel hazard metrics and fuel connectivity using Hovermap data

Two observers collected the field plot fuel hazard data in an attempt to increase the estimation accuracy, but notable differences still occurred. Tables 11 and 12 present the cover (%) and height estimates derived from the classified Hovermap point clouds for each of the fuel hazard height strata layers. When compared to near surface and elevated fuel estimates derived from visual assessments captured in the field the correlation is low (near surface RMSE = 41.46%, elevated RMSE = 44.34%).

Table 11. The mean and standard deviation of fuel height estimates derived from Hovermap point clouds for the near surface (<0.6m), elevated (0.6m – 3m), sub-canopy (3m – 5m), and canopy (>5m) strata layers.

Plot	Near Surface		Elevated		Sub-Canopy		Canopy	
	Mean	SD	Mean	SD	Mean	SD	Mean	SD
1384_FI1_hc	0.27m	0.11m	0.77m	0.46m	3.56m	0.99m	15.58m	05.18m
18553_I0_a	0.24m	0.11m	0.76m	0.68m	3.48m	1.04m	15.80m	05.74m
20736_FI1_a	0.24m	0.11m	1.14m	0.75m	2.93m	1.06m	20.31m	09.07m
26412_FI1_ec	0.28m	0.11m	0.78m	0.54m	3.58m	0.86m	23.85m	08.25m
26739_I0_a	0.25m	0.10m	1.19m	0.78m	3.37m	0.96m	28.88m	09.91m
25703-02_FI1_bc	0.26m	0.11m	1.50m	0.70m	3.26m	0.95m	24.03m	10.41m

Table 12. Fuel cover estimates derived from Hovermap point clouds for the near surface (< 0.6m), elevated (0.6m – 3m), sub-canopy (3m – 5m), and canopy (>5m) strata layers. Values are expressed as percentage of total plot size.

Plot	Near Surface (%)	Elevated (%)	Sub-Canopy (%)	Canopy (%)
1384_FI1_hc	7.4	86.3	10.7	75
18553_I0_a	43.8	47.6	19.2	88.1
20736_FI1_a	9.7	76	19.9	52.6
26412_FI1_ec	11.4	79.3	15.4	87.8
26739_I0_a	15.9	54.2	38.3	88.6
25703-02_FI1_bc	4.5	60.1	40.3	69.2

Figure 22 presents a cross section taken from plot 18553_I0_a depicting how the layer pouring algorithm classifies voxels based on their strata class and connectivity.

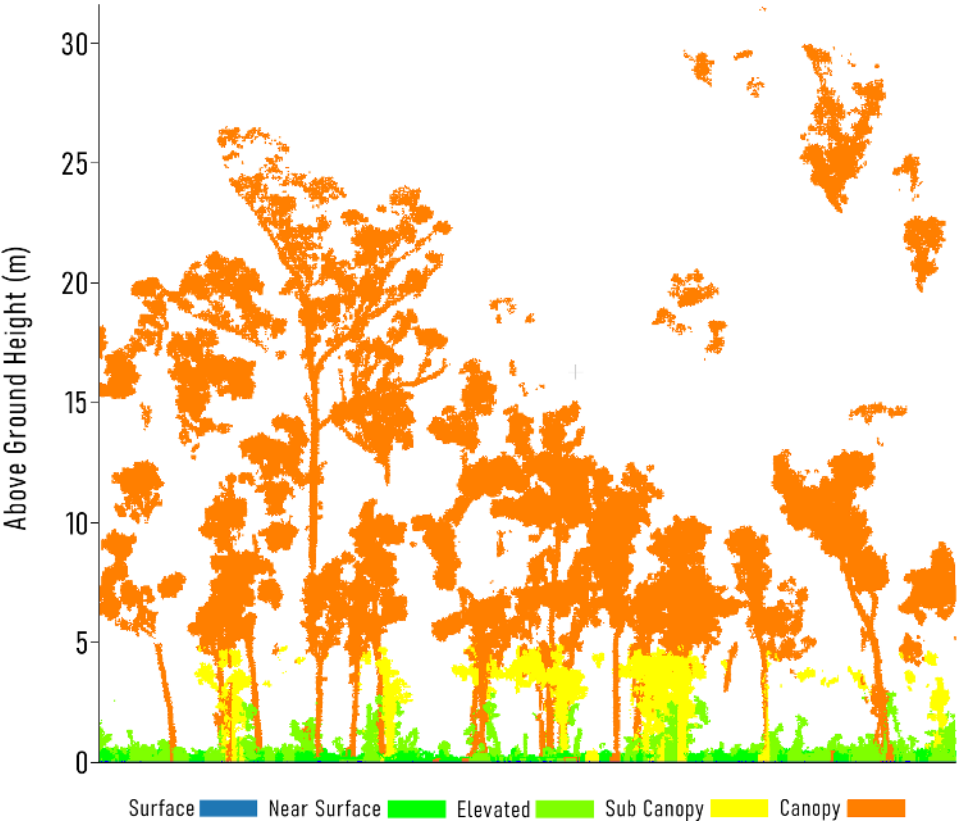


Figure 22. Cross section of a 2.5 m width transect taken from plot 18553_I0_a depicting how the vegetation strata layers of near surface (<0.6 m), elevated (0.6 m – 3 m), sub-canopy (3 m – 5 m), and canopy (>5 m) are passed down through vertically connected voxels

An example of the vertical connectivity assessment is presented in Figure 23, depicting the distribution of classified voxels across the fuel strata classes for plot 25703-02_FI1_bc. This plot also had the highest lower storey canopy cover (%) estimate (Table 6).

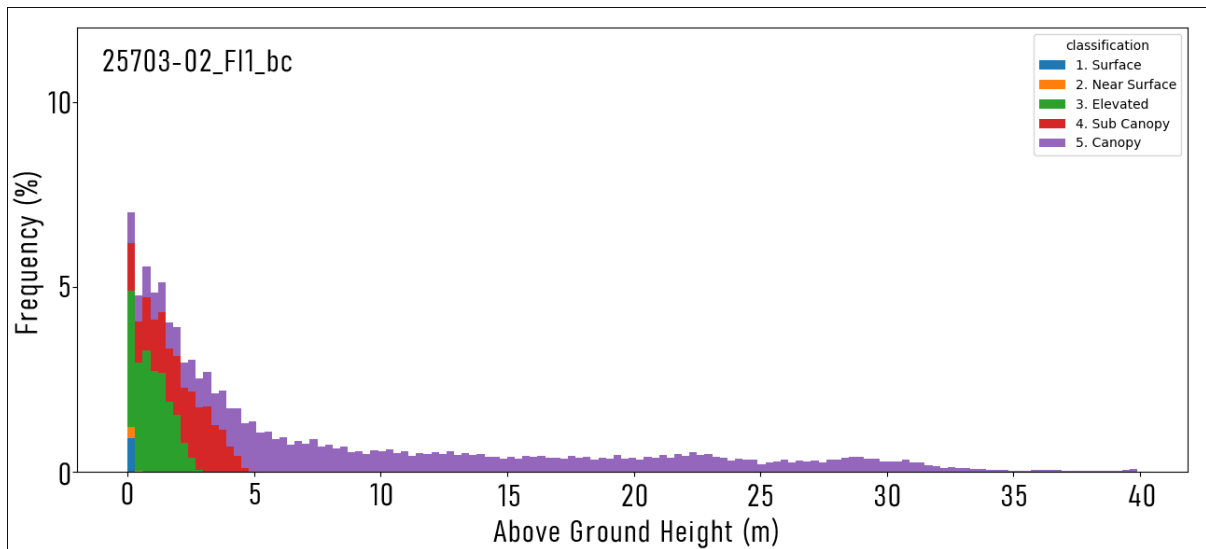


Figure 23. Above ground height distribution of filled voxels (4 cm) from the respective fuel layers within plot 25703-02_FI1_bc captured by the Hovermap

Evaluation of GEDI data for characterising forest structure changes following wildfire

Figure 24 shows the change across all relative height (RH) metrics from 2020 to 2021 in each of the fire severity classes. Negative values indicate a decline in RH. The results show a decline in RH metrics in moderate, high and extreme fire severity classes, particularly in the RH80 to RH95 metrics, where the median RH experienced a decline of up to 1 m. Lower strata RH values indicated a much smaller decline. In the low and unburnt classes, the median change in all RH values was close to zero.

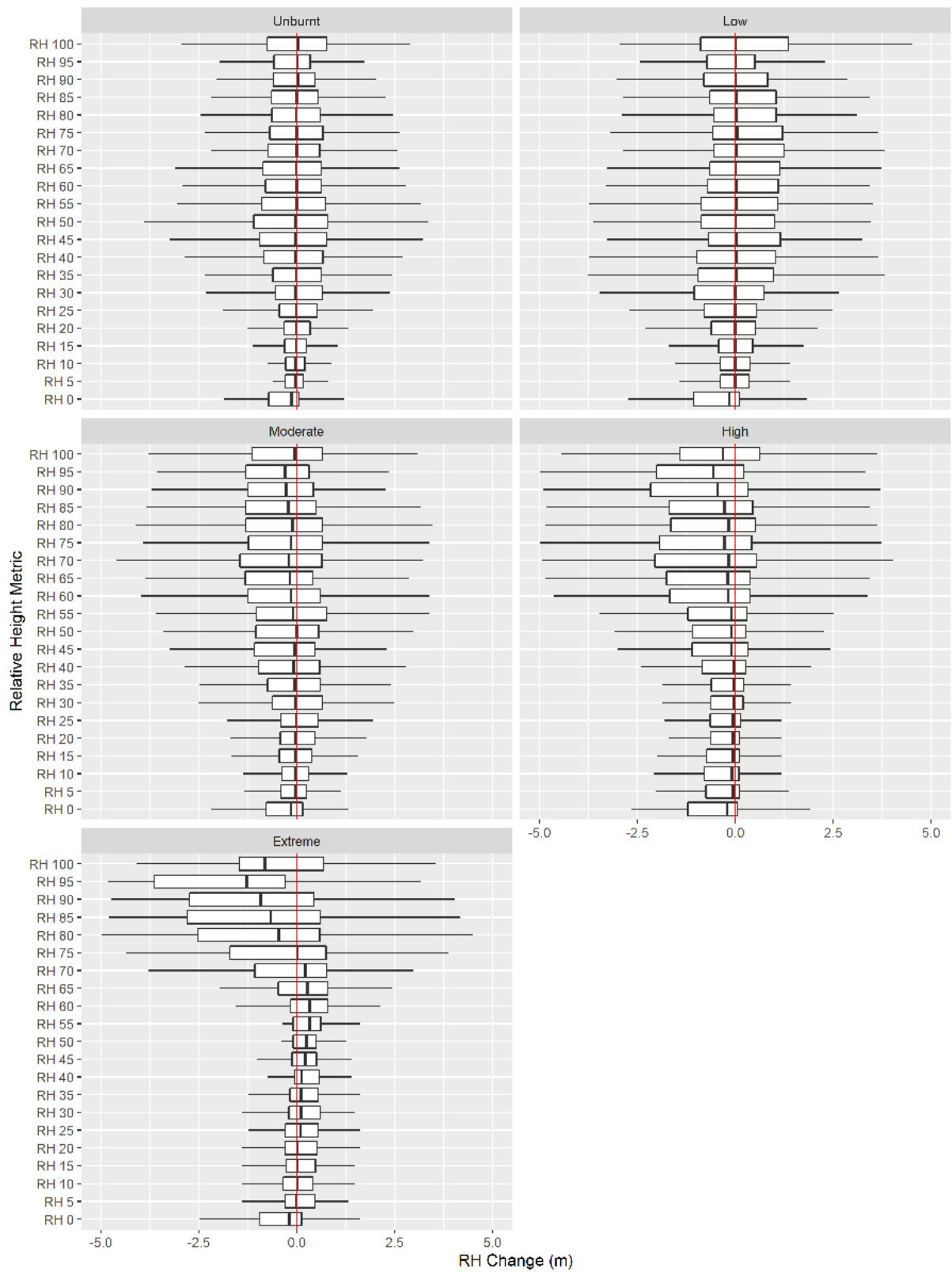


Figure 24. Change across simulated GEDI RH metrics between 2020 and 2021 in each fire severity class. Negative values indicate a decline in forest height

Discussion

Although ALS systems can cover thousands of hectares of forest there is also a need for on-ground reference data to train prediction models and collect information that cannot be measured well from above the canopy. The manual assessment of moist native eucalypt forests, however, is physically demanding, time consuming and often imprecise. Visual estimations of cover and density of vegetation strata within a native forest stand is particularly challenging, with significant variation between observers reported (Ashcroft *et al.* 2014). In addition, there is often substantial variation within stands and plots. For example, in this study, the five-point assessments of canopy cover for each plot produced significant variation in both the visual strata-level estimates and the overall canopy cover obtained using the ‘% Cover’ application. It is also acknowledged that the field measurement of tree heights using a Vertex can be imprecise in native eucalypt forests, especially in burnt plots having dense understorey regrowth and many trees presenting irregular crowns and epicormic growth. Dense understorey also hinders gathering tree location based on compass bearing and distance measurements. Therefore, field measured tree location and height may not be a good source of ground-truthing. Lidar technology, on the other hand, appears well suited to improving both the accuracy and efficiency in acquiring reference data for predicting wall-to-wall estimates.

Numerous studies have evaluated both ALS and MLS point cloud data for forest assessment although few have been undertaken in native eucalypt forests (ref. references in the Introduction). Interpine Innovation have successfully developed operational workflow solutions for obtaining tree diameter and height measurements using the MLS Hovermap unit in *Pinus radiata* plantations, but prior to this study, the capability of the technology has not been evaluated in more structurally complex eucalypt forests.

Tree-level analyses

The manual matching of field trees and with the extracted Hovermap trees for 3 of the field plots processed by Interpine Innovation revealed good correspondence for stem diameters and tree heights (Table 4), although omission errors for small diameter trees were apparent in the inventory data (Figure 9), noting that field crews did not collect information for trees with DBH < 10 cm. In an earlier study Gianneti *et al.* (2018) were not able to segment tree stems smaller than 10 cm DBH using the ZEBI hand-held scanner. Improvement in the accuracy of stem counts may be achieved through optimising the MLS survey pathway. Del Perugia *et al.* (2019), for example, examined the influence of MLS scan density on the estimation of single-tree attributes and reported that the number of trees was influenced by the survey path taken.

The challenges of tree level measurement from MLS data in complex stands with dense understorey have been highlighted in several overseas studies. Liang *et al.* (2018) evaluated the performance of a back-pack MLS and reported an increasing relative RMSE% of DBH estimates in plots classed as ‘easy’, ‘medium’ and ‘difficult’ in terms of tree density and understorey growth. Hyypä *et al.* (2020) also used a backpack MLS and reported DBH estimation error ranges of approximately 1.0 cm in ‘easy’ forests and 2.5 – 4.0 cm in ‘moderate’ to ‘difficult’ forest plots while Vatandaşlar & Zeybek (2021) reported both over- and underestimation of tree-level attributes using a hand-held Zeb-Revo (GeoSLAM) in their

more ‘difficult’ plots. Liang *et al.* (2018) concluded that the accuracy of single tree attributes, using MLS data decreased as forest complexity increased due to reduced positioning accuracy, decreased accessibility of the plot, data coverage and increased occlusion effects. This study demonstrated a good correspondence between large trees (DBH > 30 cm) measured by the inventory crew and with the Hovermap. Due to the understorey vegetation impeding both the manual and Hovermap measurements, further work is required to identify the source and type of errors associated with smaller trees. However, preliminary visual examination of two plots having higher stem counts in the Hovermap data relative to the manual estimates did not reveal any SLAM slippage/point cloud issues.

Our results show a close correspondence between the field measurements of the dominant trees and the Canopy Height Models derived from both the Hovermap and ALS data. However, while the initial application of the FSCT resulted in acceptable estimates of tree DBH, it failed to accurately estimate tree height from the Hovermap data, particularly for sub-canopy trees. To address this problem, we present a novel, significant improvement to the detection and segmentation of individual trees using a workflow based on the interpretation of Plant Area Density profiles generated from the Forest Structural Complexity Tool (FSCT) outputs (Krisanski *et al.* 2021). Quantitative assessment of the tree-level PADs permitted the identification of canopy trees versus sub-canopy trees (Figure 13). The detection and segmentation of trees from these two separated strata significantly improved tree height estimations (Figure 14). In addition, by comparing foliage only and stem only PAD point clouds it was possible to identify and count stag trees (Figure 15, Table 5).

Through this novel analysis, the Hovermap sensor provided smaller tree level differences in tree height and diameters than have been reported in other studies. For example, Cabo *et al.* (2018), using a hand-held Zeb-REVO, and Gianneti *et al.* (2018), using a ZEB1, both reported that tree height estimation was hindered for trees taller than 15 – 20 m due to the limited range of the MLS instruments. Donager *et al.* (2021) also claimed that the direct extraction of individual tree heights from CHMs is largely inadequate when sub-dominant canopy layers exist and dense conditions commonly make it unclear which heights relate to which trees. While it is acknowledged that tree segmentation algorithms using MLS data are continuing to improve (Lui *et al.* 2021), the workflows we developed resulted in significant improvements over current methods and may have broader potential for lidar-based applications in native forests. The approach of using PADs to identify overstorey and sub-canopy trees was also successfully applied to ALS data (Figure 16 a & b), enabling the production of tree crown maps for both overstorey trees and sub canopy vegetation.

Plot level analyses

Comparisons were undertaken to show the differences between the ALS and Hovermap (normalised using 10 cm voxels) plot-level datasets, but no accuracy assessment was attempted due to the truth being uncertain. While there was a third source of information based on manual field assessment, it is well known that for certain measurements lidar has superior accuracy. It is highly recommended that in future studies co-incident TLS data is also acquired to be used as a reference baseline for evaluation. Nevertheless, a close correspondence in tree heights was also obtained in the comparison of height metrics derived from the ALS and voxelised MLS point clouds (Table 9, Figure 21). In contrast, a recent

study by Donager *et al.* (2021) in Ponderosa pine forests reported that both the TLS and MLS produced less reliable canopy heights than those derived from ALS data.

Our results showed that canopy top height (p95) was uniformly higher in the ALS for all but one of the 44 subplots investigated, which was expected given the sensor position. Average height was also generally higher in the ALS, but this is more variable and increases where trees are taller. The density of points (the percentage of points above 2m) was generally higher in the Hovermap data, which could be a function of both point density and the voxelisation process. If looking only at the raw number of Hovermap points, there are a huge number of returns under 2 m in height. However, voxelisation gives equal weight to voxels with many points to those with few. The coefficient of variation was generally higher in the MLS data, as was the skewness. Positive skewness may indicate a sparser canopy and denser understory. The kurtosis did not favour either dataset and had a much lower correlation than the other metrics. The comparison of cover in each height class revealed that cover was much higher in the MLS data in all classes. This likely reflects the overall higher point density of the MLS data. It is potentially an over-estimation, which could be accounted for by removing voxels containing few points. Except for one plot (heavily burnt 20736FI1a), the ALS favoured the upper canopy, reflecting the position of the sensor and its limitations in penetrating the upper canopy.

It is clear from this analysis that the Hovermap data captures different elements of forest structure than the ALS. The Hovermap data suggests that the forest structure in these plots is likely more complex, particularly in the lower and mid stories, than the ALS suggests. Whether this can be generalised across all southeast Australian forests is unknown. A more extensive forest monitoring plot network would be necessary to confirm this. It is not yet apparent how best to combine the two datasets to get an accurate representation of plot-level structure. ALS can offer wall-to-wall information, whereas the MLS could only be considered a sampling tool akin to traditional field measurements. Therefore, the MLS information could enhance field measurements and be used for spatial modelling to impute traditional inventory metrics (e.g., basal area, above ground biomass) across the full ALS extent. The MLS may also prove useful for collecting multi-temporal information for applications such as post-disturbance recovery.

A rotational shift was required to align both the field located trees with the Hovermap point clouds as well as the Hovermap and ALS point clouds and this was evident, to a greater or lesser degree, in all plots. It is assumed that the ALS is the more accurate dataset in terms of absolute spatial position. Although the Hovermap data can potentially be realigned in post-processing, there are steps in the field that could be undertaken to aid this process, such as collecting dGPS at cardinal points (at least one) along with the plot centre. However, the issue of achieving accurate spatial co-registration of data acquired from various platforms remains a challenge due to the inherent differences in locational accuracy of the different sensors. In future studies it is highly recommended that attention be paid to improving the installation of reference markers (e.g., reflective ground control points) as well as evaluating the use of reflective paint on tree stems for numbering and DBH lines.

Fuel assessments

The results of the comparison between the Overall Fuel Hazard Assessment Guide (OFHAG) observations and the cover estimates derived from the Hovermap point clouds showed poor correlation when predicting both near-surface vegetation cover ($r^2=0.46$, RMSE = 41.5%) and vegetation cover at the elevated layer ($r^2=0.16$, RMSE = 44.3%). However, these results were not unexpected, due to the nature of visual assessment approaches and the difficulty associated with accurately estimating vegetation characteristics over a 0.1 ha plot. Visual assessment accuracy is also highly dependent on the experience of the field operators conducting the assessment and the structural complexity, density and composition of the forest environment being assessed (Watson *et al.* 2012, Volkova *et al.* 2016).

Nevertheless, this study has indicated that Hovermap point clouds were able to provide a connectivity assessment using the layer pouring algorithm by Hillman *et al.* (2011) to identify potential fuel ladders and classify voxels into strata layers. However, challenges remain within this approach as it is difficult to accurately separate points that originate from different strata layers when they are located along one of the layer boundaries. Furthermore, the algorithm biases vertical connectivity over horizontal, resulting in some cases where a cluster of voxels is connected horizontally to another from a higher class, but the classification is not passed across. Whilst this method can provide a visual representation of potential fuel ladders, and the classification of voxels can be used to extract further metrics relating to fuel hazard, there is still no metric that can be used to define the overall structural connectivity of a plot to allow for ease of intercomparison.

Fusion of point clouds from multiple platforms

Neither ALS nor TLS / MLS systems can provide complete information on the vertical structure of forests. Results from this study suggest that the ALS and Hovermap systems are more suited to different applications, due to one system operating from above the canopy and one system from below. Therefore, it is tempting to form the conclusion that, together, they describe forest structure more completely than either system in isolation. However, there are significant challenges to overcome to use and interpret the combined data properly.

Nevertheless, this study has demonstrated that when the point clouds are accurately co-registered or trees accurately matched, the Hovermap sensor can measure tree stems and understorey elements in finer detail than can be achieved by either manual/visual assessment or ALS data. At present, because of the complexity and irregularity of native forests, current multiplatform data fusion still involves substantial manual effort, but researchers overseas are now evaluating approaches to fuse multiplatform lidar datasets in forest environments (Giannetti *et al.* 2018, Guan *et al.* 2021). Donager *et al.* (2021), for example, successfully fused MLS (hand-held GeoSLAM Zeb Horizon scanner) to match an ALS dataset by initially manually shifting the MLS point cloud data before using an iterative closest point algorithm.

Coops *et al.* (2022) advocate linking lidar metrics with broad-area predictors derived from spaceborne platforms such as the GEDI (Global Ecosystem Dynamics Investigation) on board the International Space Station. Plot-level lidar metrics can be used in estimation approaches that could involve hybrid or model-based inference from hierarchical modelling.

In our study, the results from the analysis of simulated GEDI observations in post-fire recovery areas were somewhat unexpected. Relative height metrics, particularly in upper canopy, showed a decline for areas that were burnt at moderate or greater severity, despite anticipated forest regrowth. In the extreme class, this is particularly pronounced in the RH 80 to RH 95 metrics and, interestingly, this class showed an increase in the RH 40 to RH 70 metrics. The results suggest that the initial recovery following the 2019–2020 wildfires (i.e., the first few months) may have been more pronounced in the upper canopy, which was then followed by more regrowth in the lower and mid-stories as recovery progressed. This is an important finding and demonstrates how spaceborne lidar has the potential to increase our understanding of the dynamic nature of forests. Further research should be undertaken to confirm and further investigate these findings. It is recommended that the analysis should be extended over a much broader area to see whether these patterns are similar in other regions. A broader area would also enable real GEDI data to be used. ALS data should be considered as a source of validation.

Future research

It is recommended that a study comparing coincident TLS and Hovermap datasets captured within the same plots be undertaken to provide greater insight into the accuracy of the Hovermap for quantifying tree- and plot-level structural attributes, including fuel hazard metrics. Having a survey-grade representative 3D dataset to act as a truth would also allow for the exploration of possible error sources, such as the walking path and loop closure points used to move the Hovermap through the plot. Over-sampling with Hovermap may lead to increased noise whereas under-sampling may result in occluded space. For the operational adoption of this technology in native forest environments, a set of guidelines should be developed, which covers elements such as the distance between each ‘pass’ of the sensor through the plot, how frequent each loop closure should be to account for inertial drift in the positional accuracy and at what speed the sensor should be moved.

Conclusions

While numerous studies have evaluated MLS technology in plantations or relatively simple native forests, far fewer studies have been conducted in complex forests, particular eucalypt forests. Our scoping study has demonstrated that the Hovermap sensor can measure tree stems and understorey elements in more detail than can be achieved by either manual/visual assessments or ALS data. The estimation of tree height, in particular, was significantly improved through the application of a novel approach to the detection and segmentation of individual trees using a workflow based on the interpretation of Plant Area Density profiles generated from FSCT outputs. Quantitative assessment of the tree-level PADs permitted the identification of canopy trees versus sub-canopy trees. The detection and segmentation of trees from these two separated strata significantly improved tree height estimates. In addition, by comparing foliage only and stem only PAD point clouds it was possible to identify and count stag trees.

At the plot scale, there were notable differences between the inventory and Hovermap results for stem counts, most notably for trees with DBH < 30 cm, however these differences were less pronounced for basal area, because most missed stems were in the smallest diameter classes. The differences varied between plots and appeared to be influenced by understorey density and terrain.

While both ALS and MLS systems are based on lidar, the different position of the sensor in relation to the forest canopy leads to different outputs. Understanding the strengths and weaknesses of these remote sensing systems is essential prior to forming conclusions about stand structure. It is advisable to correct for the inherent heterogeneity of pulse density in the MLS point clouds and one approach is to normalise the point cloud using voxels. A 10 cm voxel was used for much of this work, except for the fuel hazard assessment, which used a smaller 4 cm voxel due to the nature of fine fuel assessments.

A direct comparison of plot-level ALS and Hovermap height distribution metrics revealed a close correspondence for p99 and p95, with the ALS values only slightly higher than the Hovermap values. As expected, ALS skewness values were negative (left skewed), indicating the data was dominated by the upper storey, while for the Hovermap data, all the skewness values were positive, indicating the influential presence of the understorey. There appears to be a cross-over point at around 10m where the ALS picks up less and the MLS more, comparatively speaking.

The Hovermap point clouds were also evaluated in terms of their ability to quantify fuel hazard, particularly the vertical connectivity between the strata layers. This preliminary evaluation demonstrated that Hovermap point clouds show promise in this regard, however further work is needed to optimise parameters and workflows, including a comparison with TLS data.

Recommendations

This 12-month study was only intended to be a proof of concept. It has, however, demonstrated that MLS technology has the capacity to improve the efficiency and accuracy of structural information sought by native forest managers. The operational fusion of point cloud data acquired by multiple platforms is also desirable. Below are recommendations for future research:

- The acquisition of coincident TLS and Hovermap MLS datasets captured within the same plots, for improved insight into the accuracy of the Hovermap sensor for quantifying tree- and plot-level structural attributes.
- Evaluation of walking survey patterns and pace of acquisition under varying understorey densities and local topographies.
- Future captures should also aim to improve co-registration of point cloud datasets through use of ground control markers and painting plot tree numbers and DBH stem bands with high reflective paint that can be detected in the lidar point clouds.
- Further research into the use of plant area density (PAD) profiles to discriminate live and dead trees in 3D point clouds.
- Evaluation of the Hovermap's ability to represent forest changes (e.g., wildfire recovery) by re-scanning plots at multiple time steps.
- Further research into the capabilities of the GEDI sensor in its abilities to characterise forest structural changes over time.

Results from these research tasks would contribute to formulating guidelines on the best use of these technologies in Australian native forests.

References

- Atkins, J.W., Bohrer, G., Fahey, R.T., Hardiman, B.S., Morin, T.H., Stovall, L. *et al.* (2018) Quantifying vegetation and canopy structural complexity from terrestrial LiDAR data using the ForestR package. *Methods in Ecology and Evolution* **9**: 2057 – 2066.
- Ashcroft M.B., Gollan, J.R. and Ramp, D. (2014) Creating vegetation density profiles for a diverse range of ecological habitats using terrestrial laser scanning. *Methods in Ecology and Evolution* **5**: 263 – 272.
- Aubry-Kientz, M., Dutrieux, R., Ferraz, A., Saatchi, H., Saatchi, S., Hamraz, H., *et al.* (2019) A comparative assessment of performance of individual tree crowns delineation algorithms from ALS data in tropical forests. *Remote Sensing* **11**: Article 1086.
- Bakx, T.R.M., Koma, Z., Seijmonsbergen, A.C. and Kissling, W.D. (2019) Use and categorization of Light Detection and Ranging vegetation metrics in avian diversity and species distribution research. *Diversity and Distribution* **25**: 1045 – 1059.
- Bienert, A., Georgi, Georgi, L., Kunz, M., von Oheimb, G. and Mass, H-G. (2021) Automatic extraction and measurement of individual trees from mobile laser scanning point clouds of forests. *Annals of Botany* **128**: 787 – 804.
- Bouvier, M., Durrieu, S., Fournier, R.A. and Renaud, J-P. (2015) Generalizing predictive models of forest inventory attributes using an area-based approach with airborne LiDAR data. *Remote Sensing of Environment* **156**: 322 – 334.
- Cabo, C., Del Pozo, S., Rodríguez – González, P., Ordóñez, C. and González-Aguilera, D. (2018) Comparing Terrestrial Laser Scanning (TLS) and wearable laser scanning (WLS) for individual tree modelling at plot level. *Remote Sensing* **10**: Article 540.
- Cakir, G.Y., Post, C.J., Mikhailova, E.A. and Schlautman, M.A. (2021) 3D LiDAR scanning of urban forest structure using a consumer tablet. *Urban Science* **5**: Article 88.
- Calders, K., Adams, J., Armston, J. and Bartholomeus, H. (2020) Terrestrial laser scanning in forest ecology: Expand the horizon. *Remote Sensing of Environment* **251**: Article 112102.
- Corrao, M.V., Sparkes, A.M. and Smith, A. (2022) A conventional cruise and felled-tree validation of individual tree diameter, height and volume derived from airborne laser scanning data of a loblolly pine (*P. taeda*) stand in Eastern Texas. *Remote Sensing* **14**: Article 2567.
- Carrasco, L., Giam, X., Papes, M. and Sheldon, K.S. (2019) Metrics of lidar-derived 3D vegetation structure reveal contrasting effects of horizontal and vertical forest heterogeneity on bird species richness. *Remote Sensing* **11**: Article 743.
- Chen, S., Liu, H., Feng, Z., Shen, C. and Chen, P. (2019) Application of personal laser scanning in forestry inventory. *PLoS ONE* **14**: e0211392.
- Ciuti, S., Tripke, H., Antikowiak, P., Silveyra Gonzalez R., Dormann C.F. and Heurich, M.Ciuti (2018) An efficient method to exploit LiDAR in animal ecology. *Methods in Ecology and Evolution* **9**: 893-904.
- Coops, N.C., Tompalski, P., Goodbody, T.R.H., Achim, A. and Mulverhill, C. (2022) Framework for near real-time for inventory using multisource remote sensing data *Forestry* **95**: 1 – 19.
- Crespo-Peremarch P., Fournier, R.A., Nguyen, V-T. van Lier, O.R. and Ruiz, L.A. (2020) A comparative assessment of the vertical distribution of forest components using full-

- waveform airborne, discrete airborne and discrete TLS data. *Forest Ecology and Management* **473**: Article 118268.
- Del Perugia, B., Giannetti, F., Chirici, G. and Travaglini, D. (2019) Influence of scan density on the estimation of single-tree attributes by hand-held mobile laser scanning. *Forests* **10**: Article 277.
- Donager, J.J., Sánchez Meador, A.J. and Blackburn, R.C. (2021) Adjudicating perspectives on forest structure – How do airborne, terrestrial and mobile Lidar-derived estimates compare? *Remote Sensing* **13**: Article 12.
- Ehbrecht, M., Schall, P., Juchheim, J., Ammer, C. and Seidel, D. (2016) Effective number of layers: A new measure for quantifying three-dimensional stand structure based on sampling terrestrial LiDAR. *Forest Ecology and Management* **380**: 212 – 223.
- Ene, L., Næsset, E. and Gobakken, T. (2012) Single tree detection in heterogeneous boreal forests using airborne laser scanning and area-based stem number estimates. *International Journal of Remote Sensing* **33**: 5171 – 5193.
- Fisher, A., Armston, J., Goodwin, N. and Scarth, P. (2020) Modelling canopy gap probability, foliage projective cover and crown projective cover from airborne lidar metrics in Australian forests and woodland. *Remote Sensing of Environment* **237**: Article 111520
- Giannetti, F., Puletti, N., Quatrini, V., Travaglini, D., Bottalico, F., Corona, P. and Chirici, G. (2018) Integrating terrestrial and airborne laser scanning for the assessment of single-tree attributes in Mediterranean forest stands. *European Journal of Remote Sensing* **51**: 795 – 807.
- Gibson, R., Danaher, T., Hehir, W. and Collins, L. (2020) A remote sensing approach to mapping fire severity in south-eastern Australia using sentinel 2 and random forest. *Remote Sensing of Environment* **240**: Article 111702
- Gollob, C., Ritter, T. and Nothdurft, A. (2020) Forest inventory with long range and high-speed personal laser scanning (PLS) and simultaneous location and mapping (SLAM) technology. *Remote Sensing* **12**: Article 1509.
- Guan, H., Su, Y., Hu, T., Wang, R., Ma, Q., Yang, Q. *et al.* (2020) A novel framework to automatically fuse multiplatform LiDAR in forest environments based on tree locations. *IEEE Transactions on GeoScience and Remote Sensing* **58**: 2165 – 2177.
- Guerra-Hernández, J., and Pascual, A. (2021) Using GEDI lidar data and airborne laser scanning to assess height growth dynamics in fast-growing species: a showcase in Spain. *Forest Ecosystems* **8**: Article 4.
- Hancock, S., Armston, M., Sun, X., Tang, H., Duncanson, L.I., Kellner, J.R. and Dubayah, R. (2019) The GEDI Simulator: A large Footprint waveform Lidar simulator for calibration and validation of spaceborne missions. *Earth Space Science* **6**: 294 – 310.
- Haywood, A. and Stone, C. (2011) Using airborne laser scanning data to estimate structural attributes of natural eucalypt regrowth forests. *Australian Forestry* **74**: 4 – 12.
- Hillman, S., Wallace, L., Lucieer, A., Reinke, K. Turner, D. and Jones, S. (2021) A comparison of terrestrial and UAS sensors for measuring fuel hazard in a dry sclerophyll forest. *International Journal of Applied Earth Observations and Geoinformation* **95**: Article 102261.
- Hyypä, E., Kukko A., Kaijaluoto, R., White, J.C., Wulder, M.A., Pyörälä, J., Liang, X., Yu, X., Wang, Y. *et al.* (2020) Accurate derivation of stem curve and volume using backpack mobile laser scanning. *ISPRS Journal of Photogrammetry and Remote Sensing* **161**: 246 – 262.

- Jiang, R. (2020) *Using LiDAR for landscape mapping of potential habitat for the critically endangered Leadbeaters possum*. PhD. Thesis, University of Melbourne.
- Juchhelm, J., Ammer, C., Schall, P. and Seidel, D. (2017) Canopy space filling rather than conventional measures of structural diversity explains productivity of beech stands. *Forest Ecology and Management* **395**: 19 – 26.
- Kandare, K., Ørka, H.O., Chan, J.C-W., and Dalponte, M. (2016) Effects of forest structure and airborne laser scanning point cloud density on 3D delineation of individual tree crowns. *European Journal of Remote Sensing* **49**: 337-359.
- Kankare, V., Liang, X., Vastaranta, M., Yu, X., Holopainen, M. and Hyypä, J. (2015) Diameter distribution estimation with laser scanning based multisource single tree inventory. *ISPRS Journal of Photogrammetry and Remote Sensing* **108**: 161 – 171.
- Karma, Y.K., Penman, T.D., Aponte, C., Hinko–Najera, N. and Bennett L.T. (2020) Persistent changes in the horizontal and vertical canopy structure of fire-tolerant forests after severe fires as quantified using multi-temporal airborne lidar data. *Forest Ecology and Management* **472**: Article 118255.
- Kim, E., Lee W-K., Yoon, M., Lee J-Y., Son, Y. and Salim, K.A. (2016) Estimation of voxel-based above-ground biomass using airborne LiDAR data in an intact tropical rainforest, Brunei. *Forests* **7**: Article 259.
- Krisanskis, S., Taskhiri, M.S., Gonzalez Aracil, S., Herries, D., Muneri, A. *et al.* (2021) Forest Structural Complexity Tool – An open source, fully-automated tool for measuring forest point clouds. *Remote Sensing* **13**: Article 4677.
- Liang, X., Kukko, A., Hyypä, J., Lehtomaki, M., Pyörälä, J., Yu, X., Kaartinen, H. Jaakkola, A. *et al.* (2018) In-situ measurements from mobile platforms: An emerging approach to address the old challenges associated with forest inventories. *ISPRS Journal of Photogrammetry and Remote Sensing* **143**: 97 – 107.
- Liu, L., Pang, Y., Li, Z. Si, L., Liao, S. (2017) Combining airborne and terrestrial laser scanning technologies to measure forest understorey volume. *Forests* **8**: Article 111.
- Liu, L., Zhang, A., Xiao, S., Hu, S., He, N., Peng, H. *et al.* (2021) Single tree segmentation and diameter at breast height estimation with mobile Lidar. *IEEE Access* **9**: 24314 – 24325.
- Mokos, M., Mikita, T., Singh, A., Tomaščík, J., Chudá, J., *et al.* (2021) Novel low-cost mobile mapping systems for forest inventories as terrestrial laser scanning alternatives. *International Journal of Applied Earth Observations and Geoinformation* **104**: Article 102512.
- Niemi, M.T. and Vauhkonen, J. (2016) Extracting canopy surface texture from airborne laser scanning data for the supervised and unsupervised prediction of area-based forest characteristics. *Remote Sensing* **8**: Article 582.
- Pearce, G.D., Watt, M.S., Dash, J.P., Stone, C. and Caccamo, G. (2019) Comparison of models describing forest inventory attributes using standard and voxel-based lidar predictors across a range of pulse densities. *International Journal of Applied Earth Observation and Geoinformation* **78**: 341 – 351.
- Pitkänen, T.P., Raunonen, P. and Kangas, A. (2019) Measuring stem diameters with TLS in boreal forests by complementary fitting procedure. *ISPRS Journal of Photogrammetry and Remote Sensing* **147**: 294 – 306.
- Potapov, P., Li, X., Hernandez-Serna, A., Tyukavina, A., Hansen, M.C., Kommareddy, A. *et al.* (2021) Mapping global forest canopy height through integration of GEDI and Landsat data. *Remote Sensing of Environment* **253**: Article 112165.

- Price, O.F. and Gordon, C.E. (2016) The potential of LiDAR technology to map fire fuel hazard over large areas of Australian forest. *Journal of Environmental Management* **181**: 663 - 673.
- Roussel, J-R., Auty, D., Coops, N.C., Tompalski, P. (2020) lidR: An R package for analysis of airborne laser scanning (ALS) data. *Remote Sensing of Environment* **251**: Article 112061.
- Sofia, S., Guglielmo, F., Maetzke, M., Coticchio, A. *et al.* (2022) The efficiency of Lidar HMLS scanning in monitoring forest structure parameters: implications for sustainable forest management. *EuroMed Journal of Business* **17**: 350-373.
- Spracklen, B. and Spracklen, D.V. (2021) Determination of structural characteristics of old-growth forest in Ukraine using spaceborne LiDAR. *Remote Sensing* **13**: Article 1233.
- Stal, C., Verbeurgt, J., De Sloover, L. and De Wulf, A. (2020) Assessment of handheld mobile terrestrial laser scanning for estimating tree parameters. *Journal of Forest Research* **32**: 1503 – 1513.
- Sumnall, M., Peduzzi, A., Fox, T.R., Wynne, R.H. and Thomas, V.A. (2016) Analysis of a lidar voxel-derived vertical profile at the plot and individual tree scales for the estimation of forest canopy layer characteristics. *International Journal of Remote Sensing* **37**: 2653 – 2681.
- Tompalski, P., Coops, N.C., White, J.C. and Wulder, M.A. (2015) Enriching ALS-derived area-based estimates of volume through tree-level downscaling. *Forests* **6**: 2608 – 2630.
- Tompalski, P., Coops, N.C., White, J.C. and Goodbody, T.R.H. (2021) Estimating changes in forest attributes and enhancing growth predictions: A review of existing approaches and future directions using airborne 3D point cloud data. *Current Forestry Reports* **7**: 1 – 24.
- Van Ewijk, K. (2015) *Estimating forest structure from LiDAR and high spatial resolution imagery for the prediction of succession and species composition*. PhD Thesis. Queens University, Canada.
- Vatandaşlar, C. and Zeybek, M. (2021) Extraction of forest inventory parameters using mobile laser scanning: A case study from Trabzon, Turkey. *Measurement* **177**: Article 109328.
- Victorian Department of Sustainability and Environment (2010) *Overall fuel hazard assessment guide*. (4th Edition) Fire and adaptive management Report no. 82.)
- Volkova, L. Sullivan, A.L., Roxburgh, S.H., and Weston, C.J. (2016) Visual assessments of fuel loads are poorly related to destructively sampled fuel loads in eucalypt forests. *International Journal of Wildland Fire* **25**: 1193 – 1201.
- Wallace, L., Gupt, V. and Jones, S. (2016) An assessment of pre- and post-fire near surface fuel hazard in an Australian dry sclerophyll forest using point cloud data captured using terrestrial laser scanner. *Remote Sensing* **8**: Article 679.
- Watson, P., Penman, S.H. and Bradstock, R.A. (2012) A comparison of bushfire fuel hazard assessors and assessment methods in dry sclerophyll forest near Sydney, Australia. *International Journal of Wildland Fire* **21**: 755 – 763.
- Wilkes, P., Jones, S.D., Suarez, L., Haywood, A., Mellor, A., Woodgate, W., Soto-Berelev, M., and Skidmore, A.K. (2016) Using discrete-return airborne laser scanning to quantify number of canopy strata across diverse forest types. *Methods and Evolution* **7**: 700 – 712.

- Wilkes, P., Disney, M., Armston, J., Bartholomeus, H., Bentley, L. et al. (2022) TLS2trees: a scalable tree segmentation pipeline for TLS data. Preprint submitted to Nature. <https://doi.org/10.1101/2022.12.07.518693>
- White, J.C., Wulder, M.A., Varhola, A., Vastaranta, M., Coops, N.C. et al. (2013) A best practices guide for generating forest inventory attributes from airborne laser scanning data using an area-based approach. *Information Report FI-X-010*. Canadian Forest Science.
- Zhang, Z., Cao, L. and She, G. (2017) Estimating forest structural parameters using canopy metrics derived from airborne LiDAR data in sub tropics. *Remote Sensing* **9**: Article 940.

Acknowledgements

We thank Adam Tyndall (NSW LLS) for funding the FCNSW inventory crew and Tom Pollard (the botanist). We also thank the FCNSW Inventory crew and Tom Pollard for their contribution to collecting the field data, Anna McConville for her QA of all the field data, Interpine Innovation for advice and guidance related to the Hovermap, Sean Krisanski for his examination of the MLS point clouds for the presence of SLAM slippage/draft and Prof Simon Jones (RMIT) for his persistence in dealing with the subcontract and invoicing.